*J. Fluid Mech.* (1988), *vol.* 194, *pp.* 391–415
*Printed in Great Britain*



# The nonlinear stability of dynamic thermocapillary liquid layers

By MARC K. SMITH
Department of Mechanical Engineering, The Johns Hopkins University, Baltimore, MD 21218, USA

(Received 31 August 1987 and in revised form 22 January 1988)

When a temperature gradient is imposed on the free surface of a thin liquid layer, fluid motion can develop due to thermocapillarity. Previous work using linear theory has shown that the layer can become unstable to a pair of obliquely travelling hydrothermal waves. Here, we shall study the nonlinear behaviour of this system to determine possible equilibrium waveforms for the instability when the critical point from the linear theory is slightly exceeded. We find that for all Prandtl numbers and small Biot numbers, possible waveforms are composed of only one of the unstable linear waves. For small Prandtl number and larger Biot numbers, a combination of the two linear waves is a possible waveform. Further analysis of these equilibrium states shows that both exhibit the Eckhaus and Benjamin–Feir sideband instability and a corresponding phase instability. Thus, they become modulated on long length- and timescales as the system develops.

## 1. Introduction

Fluid motion in a dynamic, thermocapillary liquid layer is driven by a surface-tension gradient on the fluid interface. Such a gradient appears when the temperature varies with position on the interface since surface tension is generally a non-constant function of temperature. Thermocapillary motions are important, and sometimes even dominant, in the heat and mass transfer of many systems. The manufacturing of single crystals using the float-zone method or the Czochralski method, the weld-pool behaviour during laser welding, various coating techniques, flame spreading over liquid fuels, heat transfer by dropwise condensation, and the rupture of cooling films on a heated surface are all processes in which thermocapillary flows can be important. See Scriven & Sternling (1960) and Kenning (1968) for complete reviews of such systems.

In a previous paper, Smith & Davis (1983, hereinafter referred to as SD) used a simple model to study the linear stability of a thermocapillary flow. Their model consisted of a single liquid layer bounded below by a rigid plane and above by a passive gas. A constant temperature gradient imposed on the interface gave rise to a simple velocity field in the bulk liquid through thermocapillarity. The magnitude of this temperature gradient was measured by a dimensionless Marangoni number. In their study of the linear stability of this system, SD found a new instability which they called a hydrothermal wave. The characteristics of this instability, and of several others, were described in detail. In addition, simple physical mechanisms for the instability were discussed recently by Smith (1986) and by Davis (1987). From this work, a reasonable account of the thermocapillary instabilities exhibited by this simple liquid-layer model has emerged. However, a prediction for the waveform of

the hydrothermal-wave instability is not possible because two different normal modes become unstable simultaneously when the critical Marangoni number of linear theory is attained. These modes take the form of travelling waves, one of which moves backward and to the right with respect to the surface flow of the basic state, while the other moves backward and to the left. In order to predict the waveform of the instability, we must investigate the nonlinear interactions of these unstable linear waves. Such an analysis is the subject of the present paper.

We shall use a weakly nonlinear analysis in this work valid for values of the Marangoni number that slightly exceed the critical value. Long length- and timescales are defined which describe the modulation of the complex amplitudes of the two critical modes from linear theory. This modulation is due to the presence of a finite region of unstable linear modes which appears around each of the critical modes for these slightly supercritical Marangoni numbers. The governing evolution equations for the modal amplitudes of the right and left linear waves are derived using a multiple-scale perturbation method. An analysis of this type was first used by Benney & Newell (1967) and Benney & Roskes (1969) to study waver waves and by Newell & Whitehead (1969) to study Bénard convection. The end result of the analysis in this case is a set of evolution equations which govern the behaviour of the modal amplitudes of both the right and the left linear waves as a function of time and space. In addition, two other equations appear. One governs the pressure field associated with the two critical waves and the other governs a surface heat flux which must be imposed by the environment.

There are two questions that we wish to answer in this work. First, what is the basic waveform of the nonlinear equilibrium state for this system when we slightly exceed the critical Marangoni number? Is it a pure right or left wave or is it some combination of both waves? This question is answered by considering a long-wavelength disturbance to possible nonlinear equilibrium states of the evolution equations. The second question is whether or not this nonlinear equilibrium state exhibits the sideband instability described by Eckhaus (1965) and Benjamin & Feir (1967). If it does, what is the wavelength of the most unstable disturbance?

In §2, we define the liquid-layer model, describe the basic-state solution used by SD, and derive the fundamental set of nonlinear disturbance equations. The length- and timescales which characterize the behaviour of the system just past the critical point of linear theory are defined in §3, and a perturbation analysis is then used to derive the governing nonlinear evolution equations for the modal amplitudes of the critical linear waves. These equations are analysed and discussed in terms of the linear stability of simple nonlinear equilibrium states in §4. Further discussion is given in §5 and our conclusions are presented in §6.

## 2. Problem formulation

The model used by SD is shown in figure 1. It consists of a thin liquid layer of infinite horizontal extent, bounded below by a rigid plane at $z = 0$, and bounded above by a planar interface with a passive gas at $z = d$. A Cartesian coordinate system is used with the origin located in the rigid plane and the $z$-axis directed normal to this plane. The liquid is Newtonian with constant viscosity $\mu$, density $\rho$, thermal diffusivity $\kappa$, thermal conductivity $k$, and unit thermal surface conductance $h$. The surface tension $\sigma$ of the interface varies with the temperature $T$ of the liquid according to the following approximate equation of state:

$$\sigma = \sigma_0 - \gamma(T - T_0). \tag{2.1}$$

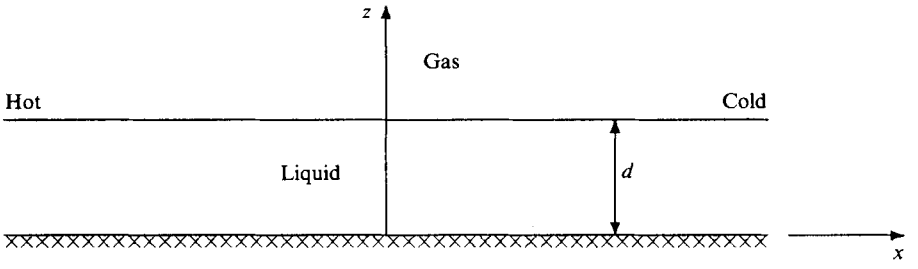


FIGURE 1. The dynamic, thermocapillary, liquid-layer model.

Here, $T_0$ is the temperature of the interface at $x = 0$, $\sigma_0$ is the surface tension at this temperature, and $\gamma = -\mathrm{d}\sigma/\mathrm{d}T > 0$ is the negative of the rate of change of surface tension with temperature.

The interface between the liquid and the gas is assumed to be nondeformable, but capable of supporting thermocapillary stresses. This assumption is tantamount to considering the limit of very large surface tension (Davis & Homsy 1980). As discussed by SD and by Smith (1986), the mechanism for the hydrothermal-wave instability considered here does not depend on the deformation of the interface. Thus, the assumption of non-deformability does not sacrifice any of the essential physics of the problem, but it does lend considerable simplification to the surface boundary conditions. To complete the model, a constant temperature gradient $\mathrm{d}T/\mathrm{d}x = -b$ is imposed along the interface of the layer and body forces are ignored.

The governing equations are scaled by referring lengths, the velocity vector $\boldsymbol{v} = (u, v, w)$, pressure $p$, temperature difference $T - T_0$, time $t$, and surface tension $\sigma$ to the scales $d$, $\gamma bd/\mu$, $\gamma b$, $bd$, $\mu/\gamma b$, and $\sigma_0$ respectively. This gives rise to the following dimensionless groups: the Marangoni number, $M = \gamma bd^2/\mu\kappa$, the Prandtl number, $Pr = \mu/\rho\kappa$, and the Biot number, $Bi = hd/k$.

The scaled equations for conservation of momentum, energy, and mass are

$$MPr^{-1}\{\boldsymbol{v}_t + (\boldsymbol{v}\cdot\boldsymbol{\nabla})\,\boldsymbol{v}\} = -\boldsymbol{\nabla}p + \nabla^2\boldsymbol{v}, \tag{2.2a}$$

$$M\{T_t + \boldsymbol{v}\cdot\boldsymbol{\nabla}T\} = \nabla^2 T, \tag{2.2b}$$

$$\boldsymbol{\nabla}\cdot\boldsymbol{v} = 0. \tag{2.2c}$$

The boundary conditions on $z = 0$ are no slip and no heat flux,

$$\boldsymbol{v} = T_z = 0, \tag{2.2d, e}$$

and the boundary conditions on $z = 1$ are for a non-deformable thermocapillary surface (see SD),

$$w = 0, \quad u_z = -T_x, \tag{2.2f, g}$$

$$v_z = -T_y, \quad -T_z = Bi\,(T - T_\infty) + Q. \tag{2.2h, i}$$

Here, letter subscripts refer to partial differentiation, $T_\infty$ is the temperature of the bounding gas far from the interface, and $Q$ is an imposed heat flux defined as positive when directed out of the layer.

The basic state of interest in this work is the return-flow solution used by SD. This solution represents the thermocapillary flow away from the ends of a long shallow

slot, and it is part of an asymptotic solution for this geometry obtained by Sen & Davis (1982). It is written as follows:

$$\bar{u} = \tfrac{3}{4}z^2 - \tfrac{1}{2}z, \quad \bar{v} = \bar{w} = 0, \tag{2.3a–c}$$

$$\bar{p}_x = \tfrac{3}{2}, \quad \bar{T} = -x + M\{\tfrac{1}{16}(1-z^4) - \tfrac{1}{12}(1-z^3)\}, \tag{2.3d, e}$$

$$\bar{T}_\infty = -x, \quad \bar{Q} = 0. \tag{2.3f, g}$$

From this basic state, we perturb the velocity, pressure, temperature, and imposed heat flux as

$$(\boldsymbol{v}, p, T, Q) = (\bar{\boldsymbol{v}}, \bar{p}, \bar{T}, \bar{Q}) + (\boldsymbol{v}', p', T', Q'), \tag{2.4}$$

and obtain the following *nonlinear disturbance* equations (for clarity, we have dropped the prime notation in these disturbance quantities):

$$M\,Pr^{-1}\{\boldsymbol{v}_t + \bar{u}\boldsymbol{v}_x + \bar{u}_z w\boldsymbol{e}_1 + (\boldsymbol{v}\cdot\boldsymbol{\nabla})\,\boldsymbol{v}\} = -\boldsymbol{\nabla}p + \nabla^2\boldsymbol{v}, \tag{2.5a}$$

$$M\{T_t + \bar{u}T_x + \bar{T}_x u + \bar{T}_z w + \boldsymbol{v}\cdot\boldsymbol{\nabla}T\} = \nabla^2 T, \tag{2.5b}$$

$$\boldsymbol{\nabla}\cdot\boldsymbol{v} = 0, \tag{2.5c}$$

$$\boldsymbol{v} = T_z = 0 \quad \text{on } z = 0, \tag{2.5d, e}$$

$$\left.\begin{aligned} u_z + T_x = 0, \quad v_z + T_y = 0, \\ w = 0, \quad T_z + Bi\,T + Q = 0, \end{aligned}\right\} \quad \text{on } z = 1. \tag{2.5f, g, h, i}$$

Here, $\boldsymbol{e}_1$ is a unit vector in the $x$-direction and all letter subscripts refer to partial differentiation.

## 3. The nonlinear stability analysis

The above system of equations (2.5) was linearized and solved in normal-mode form by SD. As discussed earlier, SD found a degeneracy in the eigenvalue at the critical point of the linear theory in that two travelling waves became unstable at the same time. Our purpose in this analysis is to investigate the nonlinear stability of the above system of equations when the Marangoni number is slightly larger than its critical value.

Following Sani (1964) and Davis & Segel (1968) we define the solution vector

$$\boldsymbol{\Psi} = (\boldsymbol{v}, p, T)^{\mathrm{T}}, \tag{3.1}$$

and write the system of disturbance equations (2.5) in matrix operator notation as

$$\mathbf{L}\boldsymbol{\Psi} = M\mathcal{N}, \tag{3.2a}$$

$$\mathbf{B}_0\boldsymbol{\Psi} = \mathbf{0} \quad \text{on } z = 0, \tag{3.2b}$$

$$\mathbf{B}_1\boldsymbol{\Psi} = -\boldsymbol{Q} \quad \text{on } z = 1. \tag{3.2c}$$

The operators and vectors used in this system are defined in Appendix A.

Next, we define the small parameter $\epsilon$ as the square root of the relative change in the Marangoni number with respect to its critical value $M_c$,

$$\epsilon^2 = \frac{M - M_c}{M_c}. \tag{3.3}$$

Then, long length- and timescales are defined in terms of $\epsilon$,

$$X_1 = \epsilon x, \quad X_2 = \epsilon^2 x, \tag{3.4a, b}$$

$$Y_1 = \epsilon y, \quad Y_2 = \epsilon^2 y, \tag{3.4c, d}$$

$$\tau_1 = \epsilon t, \quad \tau_2 = \epsilon^2 t. \tag{3.4e, f}$$

Finally, the solution is expanded as

$$\boldsymbol{\Psi} = \epsilon \boldsymbol{\Psi}^{(1)} + \epsilon^2 \boldsymbol{\Psi}^{(2)} + \epsilon^3 \boldsymbol{\Psi}^{(3)} + \ldots, \tag{3.5a}$$

$$\mathcal{N} = \epsilon^2 \mathcal{N}^{(2)} + \epsilon^3 \mathcal{N}^{(3)} + \ldots, \tag{3.5b}$$

$$\boldsymbol{Q} = \epsilon^2 \boldsymbol{Q}^{(2)} + \epsilon^3 \boldsymbol{Q}^{(3)} + \ldots. \tag{3.5c}$$

With these definitions, we now use the asymptotic technique of multiple scales to generate a sequence of problems to be solved. Details of the operator and vector expansions are contained in Appendix A and the ordered boundary-value problems are written in Appendix B.

The $O(\epsilon)$ problem is the linear problem of SD. Its normal-mode solution is

$$\boldsymbol{\Psi}^{(1)} = \boldsymbol{\Psi}_{\mathrm{R}}^{(1)} + \boldsymbol{\Psi}_{\mathrm{L}}^{(1)} + \boldsymbol{\Psi}_{\mathrm{P}}^{(1)} + \boldsymbol{\Psi}_{\mathrm{C}}^{(1)}. \tag{3.6}$$

The term $\boldsymbol{\Psi}_{\mathrm{R}}^{(1)}$ is the critical right wave with the complex amplitude $A = A(X_1, X_2, Y_1, Y_2, \tau_1, \tau_2)$ and $\boldsymbol{\Psi}_{\mathrm{L}}^{(1)}$ is the critical left wave with the complex amplitude $B = B(X_1, X_2, Y_1, Y_2, \tau_1, \tau_2)$. In these solutions, $k_{1\mathrm{c}}$ and $k_{2\mathrm{c}}$ are the wavenumbers in the $x$- and $y$-directions and $\omega_{\mathrm{c}}$ is the frequency of the oscillations. See Appendix B for details.

The third term,

$$\boldsymbol{\Psi}_{\mathrm{P}}^{(1)} = P(X_1, X_2, Y_1, Y_2, \tau_1, \tau_2)\, \tilde{\boldsymbol{\Psi}}_{\mathrm{P}}, \quad \tilde{\boldsymbol{\Psi}}_{\mathrm{P}} = \{\mathbf{0}, 1, 0\}^{\mathrm{T}}, \tag{3.7a, b}$$

represents the constant-pressure solution of the governing equations. It is important because it is modified on the long lengthscales owing to both the right and the left linear waves.

The last term is only present when $Bi = 0$. It represents a change in the average temperature of the layer which can develop when both the top and the bottom are completely insulated. It has the form

$$\boldsymbol{\Psi}_{\mathrm{C}}^{(1)} = C(X_1, X_2, Y_1, Y_2, \tau_1, \tau_2)\, \tilde{\boldsymbol{\Psi}}_{\mathrm{C}}, \quad \tilde{\boldsymbol{\Psi}}_{\mathrm{C}} = \{\mathbf{0}, 0, 1\}^{\mathrm{T}}. \tag{3.8a, b}$$

Associated with this last solution, we now impose a particular heating condition on the surface of the layer such that the average temperature perturbation of the liquid is zero. This is the condition

$$\int_V T \, \mathrm{d}V = 0, \tag{3.9}$$

where

$$\int_V (\bullet) \, \mathrm{d}V = \int_0^{2\pi/k_{c1}} \int_0^{2\pi/k_{c2}} \int_0^1 (\bullet) \, \mathrm{d}z \, \mathrm{d}y \, \mathrm{d}x. \tag{3.10}$$

Using this condition on the solution (3.6) we find that $C = 0$.

Note that because of this heating condition, the limit $Bi \to 0$ does not correspond to the upper surface of the layer being completely insulated. There must be a *non-zero* value of the surface heat flux $Q$ in order for the average temperature perturbation to be zero.

At $O(\epsilon^2)$, we have an inhomogeneous boundary-value problem that has a solution

if the forcing term is orthogonal to all adjoint solutions. Orthogonality to the adjoint right- and left-wave solutions leads to the following two equations:

$$A_{\tau_1} + \boldsymbol{c}_{\mathrm{g}}^{(+)} \cdot \hat{\boldsymbol{\nabla}}_1 A = 0, \quad B_{\tau_1} + \boldsymbol{c}_{\mathrm{g}}^{(-)} \cdot \hat{\boldsymbol{\nabla}}_1 B = 0, \tag{3.11a, b}$$

where

$$\hat{\boldsymbol{\nabla}}_1 = \boldsymbol{e}_1 \frac{\partial}{\partial X_1} + \boldsymbol{e}_2 \frac{\partial}{\partial Y_1}, \quad \boldsymbol{c}_{\mathrm{g}}^{(\pm)} = c_x \boldsymbol{e}_1 \pm c_y \boldsymbol{e}_2. \tag{3.11c, d}$$

When $Bi = 0$, orthogonality to the adjoint temperature solution yields

$$Q^{(2)} = \tfrac{1}{3} M_{\mathrm{c}} \bar{T}_x P_{X_1} + M_{\mathrm{c}} \mu (|A|^2 + |B|^2). \tag{3.11e}$$

Finally, orthogonality to the adjoint pressure solution is identically satisfied.

The use of these constraint equations ensures a solution to the $O(\epsilon^2)$ problem, which we write in the simple form

$$\boldsymbol{\Psi}^{(2)} = \boldsymbol{\Psi}_{\mathrm{A}}^{(2)} + \boldsymbol{\Psi}_{\mathrm{B}}^{(2)} + \boldsymbol{\Psi}_{\mathrm{FP}}^{(2)} + \boldsymbol{\Psi}_{\mathscr{N}}^{(2)} + \boldsymbol{\Psi}_{\mathrm{R}}^{(2)} + \boldsymbol{\Psi}_{\mathrm{L}}^{(2)} + \boldsymbol{\Psi}_{\mathrm{P}}^{(2)} + \boldsymbol{\Psi}_{\mathrm{C}}^{(2)}. \tag{3.12}$$

Here, $\boldsymbol{\Psi}_{\mathrm{A}}^{(2)}$ is a right wave that is produced through the forcing of the system by the linear right wave, $\boldsymbol{\Psi}_{\mathrm{B}}^{(2)}$ is the analogous left wave, $\boldsymbol{\Psi}_{\mathrm{FP}}^{(2)}$ is the response of the system to a pressure gradient on the long lengthscales $X_1$ and $Y_1$, and $\boldsymbol{\Psi}_{\mathscr{N}}^{(2)}$ is composed of eight different harmonic responses of the system due to the nonlinear interaction of the right and left waves and the heat flux on the surface when $Bi = 0$. The last four terms in (3.12) are the homogeneous solutions of the system. They have the same form as those of the linear problem given by (3.6), but with the amplitudes $A^{(2)}$, $B^{(2)}$, $P^{(2)}$ and $C^{(2)}$ respectively.

At $O(\epsilon^3)$, orthogonality of the forcing term to the adjoint right- and left-wave solutions results in the evolution equations:

$$A_{\tau_1}^{(2)} + \boldsymbol{c}_{\mathrm{g}}^{(+)} \cdot \hat{\boldsymbol{\nabla}}_1 A^{(2)} = h^{(+)}(A, B), \tag{3.13a}$$

$$B_{\tau_1}^{(2)} + \boldsymbol{c}_{\mathrm{g}}^{(-)} \cdot \hat{\boldsymbol{\nabla}}_1 B^{(2)} = h^{(-)}(A, B). \tag{3.13b}$$

To ensure uniformity in time for our approximation, the second-order amplitudes $A^{(2)}$ and $B^{(2)}$ must not evolve on a faster timescale than the first-order amplitudes $A$ and $B$. Therefore, $h^{(+)} = 0$ and $h^{(-)} = 0$. These conditions are equivalent to the two evolution equations:

$$A_{\tau_2} + \boldsymbol{c}_{\mathrm{g}}^{(+)} \cdot \hat{\boldsymbol{\nabla}}_2 A = \hat{L}^{(+)} A + cA + A[c_{aa}|A|^2 + c_{bb}|B|^2] + A \boldsymbol{c}_p^{(+)} \cdot \hat{\boldsymbol{\nabla}}_1 P, \tag{3.14a}$$

$$B_{\tau_2} + \boldsymbol{c}_{\mathrm{g}}^{(-)} \cdot \hat{\boldsymbol{\nabla}}_2 B = \hat{L}^{(-)} B + cB + B[c_{aa}|B|^2 + c_{bb}|A|^2] + B \boldsymbol{c}_p^{(-)} \cdot \hat{\boldsymbol{\nabla}}_1 P, \tag{3.14b}$$

in which

$$\hat{L}^{(\pm)} = c_{xx} \frac{\partial^2}{\partial X_1^2} \pm c_{xy} \frac{\partial^2}{\partial X_1 \partial Y_1} + c_{yy} \frac{\partial^2}{\partial Y_1^2}, \tag{3.14c}$$

$$\hat{\boldsymbol{\nabla}}_1^2 = \frac{\partial^2}{\partial X_1^2} + \frac{\partial^2}{\partial Y_1^2}, \quad \hat{\boldsymbol{\nabla}}_2 = \boldsymbol{e}_1 \frac{\partial}{\partial X_2} + \boldsymbol{e}_2 \frac{\partial}{\partial Y_2}, \tag{3.14d, e}$$

$$\boldsymbol{c}_p^{(\pm)} = c_{px} \boldsymbol{e}_1 \pm c_{py} \boldsymbol{e}_2. \tag{3.14f}$$

Orthogonality to the adjoint pressure solution results in the equation

$$0 = \tfrac{1}{3} \hat{\nabla}_1^2 P + \boldsymbol{c}_{rp}^{(+)} \cdot \hat{\boldsymbol{\nabla}}_1 |A|^2 + \boldsymbol{c}_{rp}^{(-)} \cdot \hat{\boldsymbol{\nabla}}_1 |B|^2, \tag{3.14g}$$

with

$$\boldsymbol{c}_{rp}^{(\pm)} = c_{rpx} \boldsymbol{e}_1 \pm c_{rpy} \boldsymbol{e}_2. \tag{3.14h}$$

| | | | $Bi = 0$ | | | |
|---|---|---|---|---|---|---|
| $Pr$ | 0.001 | 0.01 | 0.1 | 1.0 | 10.0 | $\infty$ |
| $k_{c1}$ | 0.017 | 0.055 | 0.215 | 1.052 | 2.394 | 2.446 |
| $k_{c2}$ | 0.076 | 0.236 | 0.632 | 1.498 | 0.922 | 0.335 |
| $\sigma_c$ | 0.005731 | 0.01776 | 0.04629 | 0.1048 | 0.1534 | 0.1537 |
| $M_c$ | 1.9615 | 6.2917 | 22.365 | 116.02 | 273.74 | 398.47 |
| | | | $Bi = 1.0$ | | | |
| $Pr$ | 0.001 | 0.01 | 0.1 | 1.0 | 10.0 | $\infty$ |
| $k_{c1}$ | 0.060 | 0.169 | 0.312 | 1.152 | 2.371 | 2.413 |
| $k_{c2}$ | 1.284 | 1.134 | 1.029 | 1.622 | 0.981 | 0.502 |
| $\sigma_c$ | 0.005662 | 0.01754 | 0.04769 | 0.1028 | 0.1506 | 0.1509 |
| $M_c$ | 7.0699 | 19.265 | 39.745 | 130.13 | 286.25 | 419.43 |

TABLE 1. Critical values of the wavenumber, frequency, and the Marangoni number for the linear theory of SD.

Finally, orthogonality to the adjoint temperature solution determines $Q^{(3)}$. Since we are only interested in the behaviour of the leading-order terms, we shall omit the evaluation of this condition.

The evolution equations (3.11) and (3.14) are the final set of six equations which govern the behaviour of the complex modal amplitudes of the right and left linear waves and the amplitudes of the associated pressure field and the surface heat-flux as the system is driven just above the critical point of the linear theory.

### 3.1. *Coefficient evaluation*

The evolution equations derived above are partial differential equations with constant coefficients. All of these coefficients are complex except for $c_g^{(\pm)}$, $c_{rp}^{(\pm)}$ and $\mu$ which are real. Each coefficient is evaluated by implementing the appropriate orthogonality conditions numerically. We used the program SUPORT written by Scott & Watts (1975, 1977) as our basic integrating routine for the solution of the required boundary-value problems. Briefly, this code uses a variable-step-size integrator, a shooting method, the technique of superposition, and orthonormalization. Additional code using a secant method was written by the author in order to iterate on the eigenvalue of the $O(\epsilon)$ system.

The integrals in the orthogonality conditions were done using a Simpson's integration routine. It was found that 101 points in the eigenfunctions were enough to obtain sufficient accuracy in this integration.

The coefficients of the evolution equations were calculated for twelve different parameter sets. These covered a complete range of Prandtl numbers and two different Biot numbers. The critical values of the wavenumber vector, frequency, and the Marangoni number are shown in table 1. Note that these computations supplement the linear stability results of SD in two ways. First, the calculations for $Bi = 1$ were not included in that work. Second, the above values for the critical wavenumbers are accurate to three decimal places. This kind of accuracy was required in order to obtain sufficient accuracy in the coefficients of the evolution equations. Representative values for the coefficients of the evolution equations (3.11) and (3.14) are shown in table 2(*a* and *b*).

The linear theory of SD expressed in the $O(\epsilon)$ problem can be used to calculate the

(*a*) $Bi = 0$

| $Pr$ | 0.01 | 1.0 | $\infty$ |
|---|---|---|---|
| $c_x$ | $(0.4037 \times 10^{-1},\ 0.8082 \times 10^{-4})$ | $(0.2454 \times 10^{-1},\ -0.2238 \times 10^{-4})$ | $(-0.2000 \times 10^{-1},\ 0.1400 \times 10^{-4})$ |
| $c_y$ | $(-0.6279 \times 10^{-1},\ -0.2625 \times 10^{-4})$ | $(-0.6376 \times 10^{-1},\ -0.1435 \times 10^{-4})$ | $(-0.6500 \times 10^{-2},\ 0.5230 \times 10^{-6})$ |
| $c_{xx}$ | $(0.1745,\ -0.6503 \times 10^{-1})$ | $(0.3203 \times 10^{-1},\ -0.3344 \times 10^{-1})$ | $(0.1961 \times 10^{-1},\ 0.2520 \times 10^{-1})$ |
| $c_{xy}$ | $(-0.2275 \times 10^{-1},\ 0.8538 \times 10^{-1})$ | $(-0.2657 \times 10^{-1},\ 0.6335 \times 10^{-1})$ | $(-0.2198 \times 10^{-2},\ 0.5412 \times 10^{-2})$ |
| $c_{yy}$ | $(0.5139 \times 10^{-1},\ 0.6403 \times 10^{-1})$ | $(0.1485 \times 10^{-1},\ -0.8636 \times 10^{-2})$ | $(0.5743 \times 10^{-3},\ -0.9486 \times 10^{-2})$ |
| $c$ | $(0.7879 \times 10^{-2},\ -0.5015 \times 10^{-2})$ | $(0.6499 \times 10^{-1},\ -0.2288 \times 10^{-1})$ | $(0.6476 \times 10^{-1},\ -0.4519 \times 10^{-1})$ |
| $c_{aa}$ | $(-0.4171 \times 10^{-3},\ 0.1153 \times 10^{-2})$ | $(-0.2112,\ 0.2539)$ | $(-0.2549 \times 10^{+1},\ -0.2196 \times 10^{+1})$ |
| $c_{bb}$ | $(-0.1205 \times 10^{-2},\ -0.6626 \times 10^{-3})$ | $(-0.2462,\ 0.3828)$ | $(-0.4911 \times 10^{+1},\ -0.4242 \times 10^{+1})$ |
| $c_{px}$ | $(-0.2673 \times 10^{-2},\ 0.1426 \times 10^{-1})$ | $(-0.1661,\ 0.6747)$ | $(-0.2135,\ 0.1672 \times 10^{+1})$ |
| $c_{py}$ | $(0.1475 \times 10^{-2},\ 0.9078 \times 10^{-1})$ | $(-0.3063 \times 10^{-1},\ 0.5985)$ | $(-0.3886 \times 10^{-4},\ 0.1349)$ |
| $\mu$ | $-0.3087 \times 10^{-2}$ | $-0.1798$ | $-0.2410 \times 10^{-4}$ |
| $c_{rpx}$ | $0.3088 \times 10^{-2}$ | $0.1798$ | $0.5495 \times 10^{-9}$ |
| $c_{rpy}$ | $0.3754 \times 10^{-2}$ | $-0.4816 \times 10^{-1}$ | $0$ |

(*b*) $Bi = 1.0$

| $Pr$ | 0.01 | 1.0 | $\infty$ |
|---|---|---|---|
| $c_x$ | $(0.3292 \times 10^{-1},\ -0.3545 \times 10^{-4})$ | $(0.2241 \times 10^{-1},\ 0.2433 \times 10^{-4})$ | $(-0.1808 \times 10^{-1},\ -0.1452 \times 10^{-5})$ |
| $c_y$ | $(-0.7355 \times 10^{-2},\ -0.1676 \times 10^{-6})$ | $(-0.5320 \times 10^{-1},\ -0.6689 \times 10^{-5})$ | $(-0.9499 \times 10^{-2},\ -0.1086 \times 10^{-5})$ |
| $c_{xx}$ | $(0.2581,\ -0.1756)$ | $(0.3267 \times 10^{-1},\ -0.2467 \times 10^{-1})$ | $(0.2048 \times 10^{-1},\ 0.2552 \times 10^{-1})$ |
| $c_{xy}$ | $(-0.4376 \times 10^{-1},\ 0.3045 \times 10^{-1})$ | $(-0.2443 \times 10^{-1},\ 0.5326 \times 10^{-1})$ | $(-0.3676 \times 10^{-2},\ 0.7521 \times 10^{-2})$ |
| $c_{yy}$ | $(0.4524 \times 10^{-2},\ 0.4199 \times 10^{-2})$ | $(0.1436 \times 10^{-1},\ -0.7511 \times 10^{-2})$ | $(0.1296 \times 10^{-2},\ -0.8943 \times 10^{-2})$ |
| $c$ | $(0.8322 \times 10^{-2},\ -0.4173 \times 10^{-2})$ | $(0.7022 \times 10^{-1},\ -0.3006 \times 10^{-1})$ | $(0.6313 \times 10^{-1},\ -0.4669 \times 10^{-2})$ |
| $c_{aa}$ | $(-0.4410 \times 10^{-1},\ 0.1646)$ | $(-0.2412,\ 0.3160)$ | $(-0.2744 \times 10^{+1},\ -0.2272 \times 10^{+1})$ |
| $c_{bb}$ | $(-0.3439 \times 10^{-1},\ -0.8526 \times 10^{-1})$ | $(-0.3121,\ 0.5868)$ | $(-0.5083 \times 10^{+1},\ -0.4198 \times 10^{+1})$ |
| $c_{px}$ | $(-0.7515 \times 10^{-2},\ 0.5736 \times 10^{-1})$ | $(-0.1418,\ 0.7206)$ | $(-0.2191,\ 0.1644 \times 10^{+1})$ |
| $c_{py}$ | $(0.7394 \times 10^{-3},\ 0.4438)$ | $(-0.2985 \times 10^{-1},\ 0.6426)$ | $(0.8297 \times 10^{-3},\ 0.2026)$ |
| $\mu$ | — | | |
| $c_{rpx}$ | $0.7995$ | $0.2349$ | $0.1694 \times 10^{-22}$ |
| $c_{rpy}$ | $0.2875 \times 10^{-22}$ | $-0.6568 \times 10^{-1}$ | $0.0000$ |

TABLE 2. The coefficients for the evolution equations (3.11) and (3.14) for (*a*) $Bi = 0$, and (*b*) $Bi = 1.0$.

neutral surface and the associated frequency surface as functions of the wavenumbers. It can be shown that the coefficients of the linear terms in the evolution equations (3.11) and (3.14) are related to the local geometry of these surfaces at the critical point. These relations, given in Appendix C, provide an independent check on the coefficients of the linear terms of the evolution equations. Using a central-difference approximation to calculate the surface geometry from the linear problem at the critical point, we find that the coefficients are accurate to within three to four significant figures.

## 4. Linear stability of the evolution equations

Rather than integrating the evolution equations derived in the previous section for some given initial conditions, we shall now investigate the linear stability of possible equilibrium states of this set of equations. The results of this analysis will answer the questions posed in the introduction.

First, a few simplifications are in order. Since $Q^{(2)}$ only appears in (3.11*e*), we shall ignore it in the subsequent analysis. Also, the linear evolution equations (3.11*a*, *b*) and the similar first derivative terms in (3.14*a*, *b*) represent a wave motion in the

modal amplitudes of the right and left linear waves with the respective group velocities $\boldsymbol{c}_g^{(+)}$ and $\boldsymbol{c}_g^{(-)}$. As long as these amplitudes are decoupled in the evolution equations, we may redefine our space variables so that we move at the group velocity of each particular motion. Thus, for the right wave, we have

$$(X, Y) = (X_1, Y_1) - \boldsymbol{c}_g^{(+)}\tau_1, \quad (\xi, \eta) = (X_2, Y_2) - \boldsymbol{c}_g^{(+)}\tau_2, \tag{4.1a, b}$$

and for the left wave, we have

$$(X, Y) = (X_1, Y_1) - \boldsymbol{c}_g^{(-)}\tau_1, \quad (\xi, \eta) = (X_2, Y_2) - \boldsymbol{c}_g^{(-)}\tau_2. \tag{4.2a, b}$$

We shall note when this decoupling occurs in the analysis and we shall make a special transformation when it does not.

After this change in variables, the two modal amplitudes become independent of the timescale $\tau_1$. Thus, the system evolves on the timescale $\tau_2$ described by system (3.14). This is written in terms of our new variables as follows:

$$A_{\tau_2} = L^{(+)}A + cA + A\{c_{aa}|A|^2 + c_{bb}|B|^2\} + A\boldsymbol{c}_p^{(+)} \cdot \boldsymbol{\nabla} P, \tag{4.3a}$$

$$B_{\tau_2} = L^{(-)}B + cB + B\{c_{aa}|B|^2 + c_{bb}|A|^2\} + B\boldsymbol{c}_p^{(-)} \cdot \boldsymbol{\nabla} P, \tag{4.3b}$$

$$0 = \tfrac{1}{3}\nabla^2 P + \boldsymbol{c}_{rp}^{(+)} \cdot \boldsymbol{\nabla}|A|^2 + \boldsymbol{c}_{rp}^{(-)} \cdot \boldsymbol{\nabla}|B|^2. \tag{4.3c}$$

Here,

$$L^{(\pm)} = c_{xx}\frac{\partial^2}{\partial X^2} \pm c_{xy}\frac{\partial^2}{\partial X\,\partial Y} + c_{yy}\frac{\partial^2}{\partial Y^2}, \tag{4.3d}$$

$$\boldsymbol{\nabla} = \boldsymbol{e}_1\frac{\partial}{\partial X} + \boldsymbol{e}_2\frac{\partial}{\partial Y}, \quad \nabla^2 = \frac{\partial^2}{\partial X^2} + \frac{\partial^2}{\partial Y^2}. \tag{4.3e, f}$$

Our analysis of system (4.3) proceeds by first finding simple equilibrium states and then performing a straightforward linear stability analysis about these states.

### 4.1. *The null state*

The first solution that we shall examine is the null state defined as

$$A_0 = B_0 = P_0 = 0. \tag{4.4}$$

Perturbing about this state, we develop the following set of linear disturbance equations:

$$A'_{\tau_2} = L^{(+)}A' + cA', \quad B'_{\tau_2} = L^{(-)}B' + cB', \quad 0 = \tfrac{1}{3}\nabla^2 P'. \tag{4.5a–c}$$

The amplitudes of the perturbations $A'$, $B'$ and $P'$ have all decoupled in this set of equations. Thus, we can consider each disturbance separately and make the appropriate change in reference frame. Also, given the symmetry between $A'$ and $B'$, it is sufficient to consider only the $A'$-equation in order to calculate the stability of the null state.

The solution of the disturbance equation (4.5$a$) uses normal modes in the form

$$A' = \mathscr{A}E_k, \quad E_k = \exp\{\mathrm{i}(\boldsymbol{k} \cdot \boldsymbol{X}) + \lambda\tau_2\}. \tag{4.6a, b}$$

Here $\boldsymbol{k} = (k_1, k_2)$ is the disturbance wavenumber vector and $\lambda$ is a complex number composed of the growth rate $\lambda_r$ and the frequency $\lambda_i$ of the disturbance. The subscripts r and i refer to the real and imaginary parts respectively. We find that

$$\lambda = L_k^{(+)} + c. \tag{4.7}$$

The symbol $L_k^{(+)}$ is defined as follows. Given any vector $\boldsymbol{a} = (a_1, a_2)$, then

$$L_a^{(\pm)} = -c_{xx}a_1^2 \mp c_{xy}a_1a_2 - c_{yy}a_2^2. \tag{4.8}$$

This notation is used extensively in the following analysis.

One can show that $\lambda_r = L_{kr}^{(+)} + c_r = 0$ defines an ellipse which is the intersection of the plane $M = M_c(1+\epsilon^2)$ and the neutral surface for the right wave of the linear theory of SD. Thus, for $\lambda_r > 0$ ($< 0$) we are above (below) the neutral surface and the null state is unstable (stable).

### 4.2. *The pure wave*

In the next solution one of the amplitudes, $A$ or $B$, is constant and the other is zero. This corresponds to either a pure right or left wave from the linear theory of SD and we shall refer to it as the pure-wave state. Owing to the symmetry of the problem, we can obtain the same information by considering either a pure-$A$ or a pure-$B$ solution. Thus, we shall ignore the pure-$B$ solution.

The pure-wave state is given as

$$A_0 = \mathscr{A}_0 E_{\kappa_R}, \quad B_0 = 0, \quad P_0 = 0, \tag{4.9a–c}$$

where $\mathscr{A}_0$ is a complex constant defined as

$$|\mathscr{A}_0|^2 = \frac{L_{\kappa_R r}^{(+)} + c_r}{-c_{aar}}, \tag{4.9d}$$

and

$$E_{\kappa_R} = \exp\{\mathrm{i}(\boldsymbol{\kappa}_R \cdot \boldsymbol{X} + \sigma_R \tau_2)\}, \tag{4.9e}$$

$$\sigma_R = L_{\kappa_R i}^{(+)} + c_i + c_{aai}|\mathscr{A}_0|^2. \tag{4.9f}$$

This state represents a uniform wave with a change in frequency of $\sigma_R$ and a change in wavenumber of $\boldsymbol{\kappa}_R$ with respect to the critical mode of linear theory. Since $|\mathscr{A}_0|^2$ must be positive and our calculations show that $c_{aar} < 0$ for all the parameter sets considered, we have the relationship $L_{\kappa_R r}^{(+)} + c_r > 0$. This limits the values of $\boldsymbol{\kappa}_R$ to those vectors that lie inside the ellipse defined earlier, i.e. above the neutral surface from the linear theory.

We now perturb this equilibrium state,

$$A = A_0 + A', \quad B = B', \quad P = P', \tag{4.10a–c}$$

and obtain the following *linearized* disturbance equations:

$$A'_{\tau_2} = L^{(+)}A' + cA' + c_{aa}\{A_0^2 A'^* + 2|\mathscr{A}_0|^2 A'\} + A_0 \boldsymbol{c}_p^{(+)} \cdot \boldsymbol{\nabla} P', \tag{4.11a}$$

$$B'_{\tau_2} = L^{(-)}B' + cB + c_{bb}|\mathscr{A}_0|^2 B', \tag{4.11b}$$

$$0 = \tfrac{1}{3}\nabla^2 P' + \boldsymbol{c}_{rp}^{(+)} \cdot \boldsymbol{\nabla}(A_0 A'^* + A_0^* A'). \tag{4.11c}$$

The asterisk refers to the complex conjugate.

The $B'$-equation has decoupled from this system and so we solve it separately. Using the normal modes as defined in (4.6$b$), we let

$$B' = \mathscr{B} E_k, \tag{4.12}$$

and obtain

$$\lambda = L_k^{(-)} + c + c_{bb}|\mathscr{A}_0|^2. \tag{4.13}$$

The growth rate for this $B'$-disturbance is

$$\lambda_r = L_{kr}^{(-)} + c_r + |\mathscr{A}_0|^2 c_{bbr}. \tag{4.14}$$

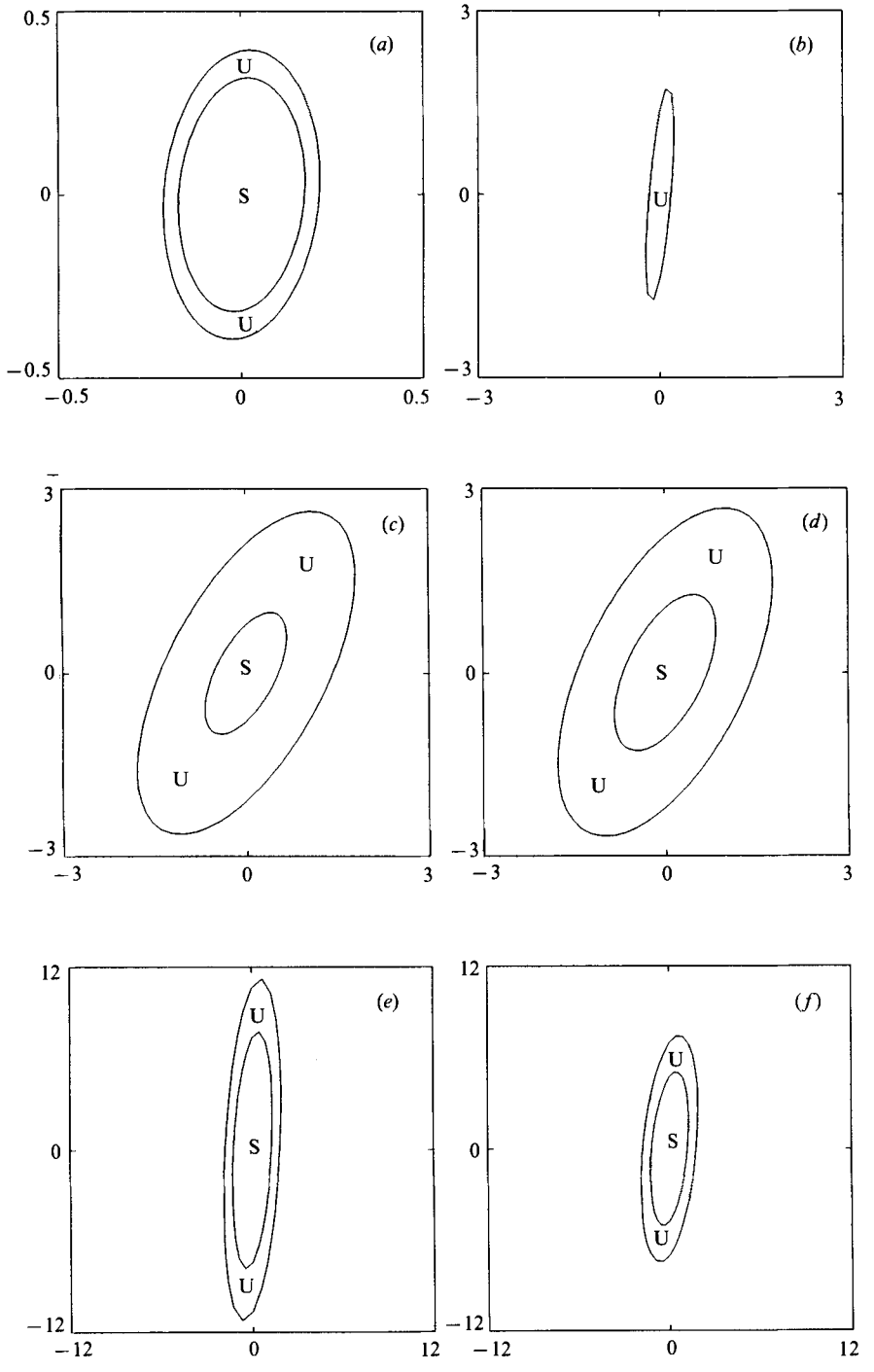


FIGURE 2. The elliptical region of possible pure-wave equilibrium states plotted in the $\kappa_R$-wavenumber space. The subregions marked with a U (an S) are unstable (stable) to a disturbance of the opposite kind. (*a*) $Pr = 0.01$ and $Bi = 0$, (*b*) $Pr = 0.01$ and $Bi = 1$, (*c*) $Pr = 1.0$ and $Bi = 0$, (*d*) $Pr = 1.0$ and $Bi = 1$, (*e*) $Pr = \infty$ and $Bi = 0$, and (*f*) $Pr = \infty$ and $Bi = 1$.

The term $L_{kr}^{(-)}$ is non-positive and its largest value for any wavenumber vector $\boldsymbol{k}$ is 0. Thus, when we consider the most dangerous $B'$-disturbance, we will have instability if

$$c_r + |\mathscr{A}_0|^2 c_{bbr} > 0. \tag{4.15}$$

Since $c_{bbr}$ is negative for all parameter sets calculated and with $|\mathscr{A}_0|^2$ defined in (4.9$d$), this relationship describes an elliptic annular region bounded on the outside by the ellipse defining the region of possible pure-$A$ equilibrium states. Representative plots of this region for several parameter sets are shown in figure 2($a$–$f$). For $Bi = 0$, there is always a region where the pure-$A$ wave is stable to a $B'$-disturbance. However, for $Bi = 1$ and $Pr = 0.001$ or $Pr = 0.01$, the $B'$-disturbance always grows.

The remaining equations for $A'$ and $P'$ can be solved using the following normal-mode forms:

$$A' = (a^{(+)}E_k + a^{(-)}E_k^*)E_{\kappa_R}, \quad P' = p_R E_k + p_R^* E_k^*, \tag{4.16$a$, $b$}$$

where $E_k$ is defined in (4.6$b$) and $E_{\kappa_R}$ is defined in (4.9$e$). After some algebraic manipulations, we obtain the determinant for the eigenvalues

$$\begin{vmatrix} f_{R+} + |\mathscr{A}_0|^2 f_{a+} - \lambda & \mathscr{A}_0^2 f_{a+} \\ \mathscr{A}_0^{2*} f_{a+}^* & f_{R-}^* + |\mathscr{A}_0|^2 f_{a+}^* - \lambda \end{vmatrix} = 0, \tag{4.17$a$}$$

$$f_{R\pm} = L_{\kappa_R \pm k}^{(+)} - L_{\kappa_R}^{(+)}, \tag{4.17$b$}$$

$$f_{a+} = c_{aa} - \frac{3(\boldsymbol{c}_p^{(+)} \cdot \boldsymbol{k})\,(\boldsymbol{c}_{rp}^{(+)} \cdot \boldsymbol{k})}{|\boldsymbol{k}|^2}. \tag{4.17$c$}$$

To determine the instability of any particular equilibrium state to an $A'$-disturbance, we must determine if $\lambda_r$ calculated from the determinant (4.17$a$) is positive for any value of $\boldsymbol{k}$. One particular disturbance of interest is $\boldsymbol{k} = \boldsymbol{0}$, the long-wave approximation. Evaluating the determinant (4.17$a$) in this limit we obtain the characteristic equation

$$\lambda(\lambda - 2|\mathscr{A}_0|^2 f_{a+_r}) = 0. \tag{4.18}$$

The first root, $\lambda = 0$, represents a neutrally stable phase change of the pure-wave equilibrium state. The other, $\lambda = 2|\mathscr{A}_0|^2 f_{a+_r}$, represents an amplitude perturbation which is unstable for any pure-wave equilibrium state if $f_{a+_r} > 0$. The value of $f_{a+_r}$ depends on the direction with which we approach the limiting value $\boldsymbol{k} = \boldsymbol{0}$ as shown in (4.17$c$). The largest value for any direction can be shown to be

$$f_{a+_r} = c_{aar} + 3|\boldsymbol{c}_{pr}^{(+)}|\,|\boldsymbol{c}_{rp}^{(+)}|\sin^2(\tfrac{1}{2}\theta), \tag{4.19}$$

where $\theta$ is the angle between the vectors $\boldsymbol{c}_{pr}^{(+)}$ and $\boldsymbol{c}_{rp}^{(+)}$.

With this result, we test all of the parameter sets used in this study and find that the amplitude mode is always stable. Thus, there is the possibility of what Kuramoto (1984) calls a phase instability in this system if the zero root becomes positive for non-zero wavenumbers. To determine this, we could find the first-order correction to the zero eigenvalue for $\boldsymbol{k} \to \boldsymbol{0}$ and check its sign. Rather than settle for this limited domain of applicability, we instead calculate $\lambda_r$ directly from the determinant (4.17$a$) for each possible equilibrium wavenumber vector $\boldsymbol{\kappa}_R$ and see if it is positive for any value of the perturbation wavenumber vector $\boldsymbol{k}$. This was done with a simple algorithm in which the values of $\boldsymbol{\kappa}_R$ were chosen on an (11pt, 6°) polar mesh superimposed on the elliptical region of possible values. For each case, a perturbation was found which made $\lambda_r > 0$. For illustration, we let $\boldsymbol{\kappa}_R = \boldsymbol{0}$ and show the regions of instability for which $\lambda_r > 0$ in figure 3($a$–$f$). The neutral boundary of each region, defined by $\lambda_r = 0$, is the outermost curve. It intersects the origin, indicating that we

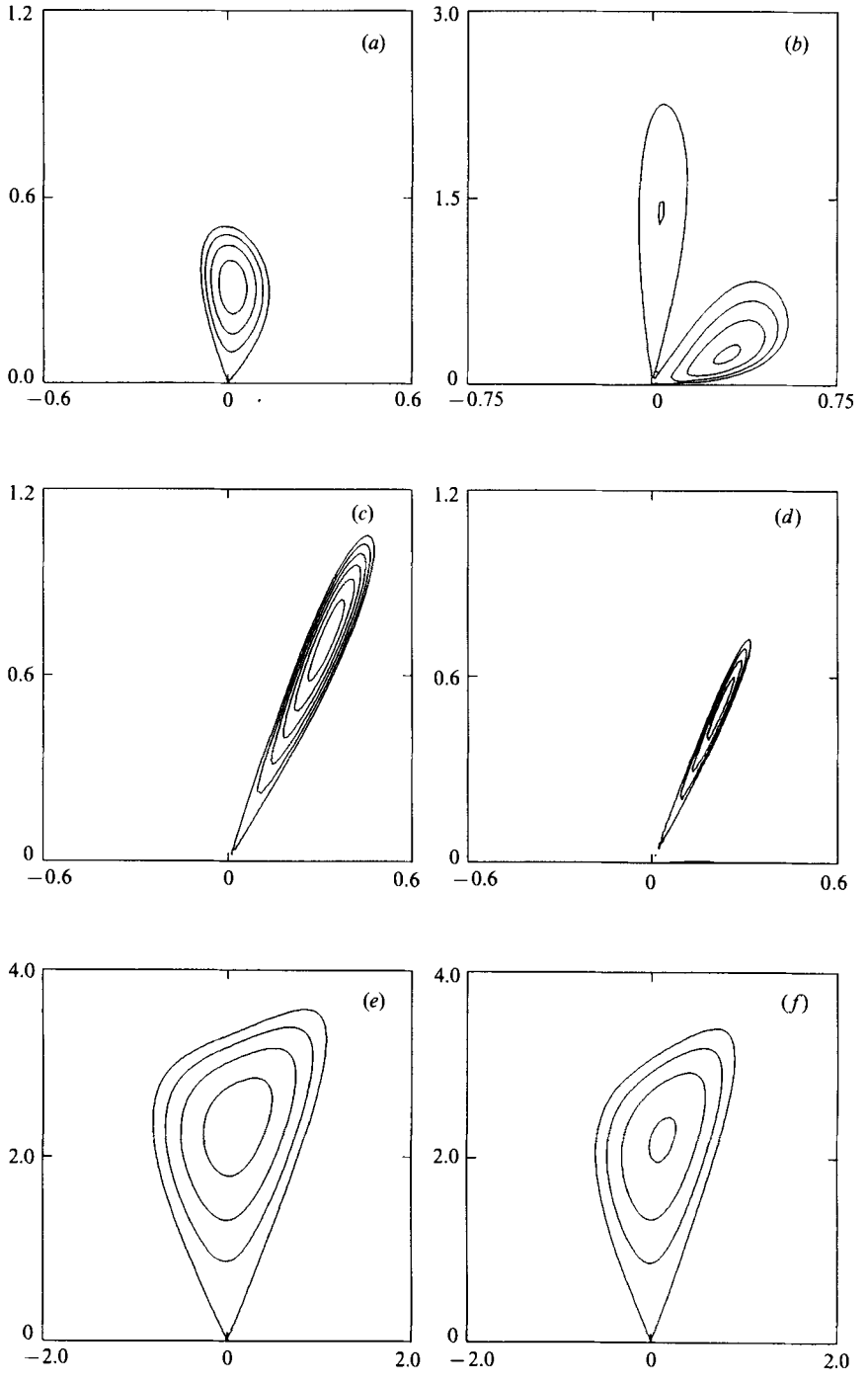


FIGURE 3. The region of sideband instability for a pure wave with $\boldsymbol{\kappa}_{\mathrm{R}} = \mathbf{0}$ plotted in the $\boldsymbol{k}$-disturbance-wavenumber space. (*a*) $Pr = 0.01$ and $Bi = 0$, (*b*) $Pr = 0.01$ and $Bi = 1$, (*c*) $Pr = 1.0$ and $Bi = 0$, (*d*) $Pr = 1.0$ and $Bi = 1$, (*e*) $Pr = \infty$ and $Bi = 0$, and (*f*) $Pr = \infty$ and $Bi = 1$.

| | | | | | | |
|---|---|---|---|---|---|---|
| | | | $Bi = 0$ | | | |
| $Pr$ | 0.001 | 0.01 | 0.1 | 1.0 | 10.0 | $\infty$ |
| $k_1$ | 0.00276 | 0.0140 | 0.0922 | 0.326 | −0.105 | 0.106 |
| $k_2$ | 0.113 | 0.315 | 0.521 | 0.723 | 1.459 | 2.356 |
| $\lambda_r$ | $0.165\times10^{-2}$ | $0.362\times10^{-2}$ | $0.166\times10^{-2}$ | $0.569\times10^{-3}$ | $0.393\times10^{-2}$ | $0.177\times10^{-1}$ |
| | | | $Bi = 1.0$ | | | |
| $Pr$ | 0.001 | 0.01 | 0.1 | 1.0 | 10.0 | $\infty$ |
| $k_1$ | 0.138 | 0.301 | 0.107 | 0.223 | −0.0848 | 0.122 |
| $k_2$ | 0.128 | 0.240 | 0.749 | 0.505 | 1.157 | 2.207 |
| $\lambda_r$ | $0.182\times10^{-1}$ | $0.189\times10^{-1}$ | $0.174\times10^{-2}$ | $0.108\times10^{-3}$ | $0.154\times10^{-2}$ | $0.124\times10^{-1}$ |

TABLE 3. The maximum value of the growth rate and the associated value of the wavenumber for the pure wave with $\boldsymbol{\kappa}_R = \mathbf{0}$.

have a phase instability near this point in which the disturbance primarily affects the phase of the pure wave. In table 3, we detail the maximum value of $\lambda_r$ and the corresponding value of $\boldsymbol{k}$ for each parameter set. These values indicate that the most dangerous disturbance does not occur at small $|\boldsymbol{k}|$. The associated eigenfunctions also show that the disturbance affects both the amplitude and the phase of the pure wave. This type of an instability, first studied by Eckhaus (1965) and Benjamin & Feir (1967), is known as a sideband instability after the form of the disturbance (4.16) used in the analysis.

### 4.3. *The mixed wave*

The last group of equilibrium solutions that we shall consider is the mixed-wave state. Here, both waves are present with the forms

$$A_0 = \mathscr{A}_0 E_{\kappa_R}, \quad B_0 = \mathscr{B}_0 E_{\kappa_L}, \quad P_0 = 0, \tag{4.20a–c}$$

where

$$|\mathscr{A}_0|^2 = \frac{c_{aar}(L^{(+)}_{\kappa_R r} + c_r) - c_{bbr}(L^{(-)}_{\kappa_L r} + c_r)}{c^2_{bbr} - c^2_{aar}}, \tag{4.20d}$$

$$|\mathscr{B}_0|^2 = \frac{c_{aar}(L^{(-)}_{\kappa_L r} + c_r) - c_{bbr}(L^{(+)}_{\kappa_R r} + c_r)}{c^2_{bbr} - c^2_{aar}}, \tag{4.20e}$$

$$E_{\kappa_R} = \exp\{\mathrm{i}(\boldsymbol{\kappa}_R \cdot \boldsymbol{X} + \sigma_R \tau_2)\}, \tag{4.20f}$$

$$E_{\kappa_L} = \exp\{\mathrm{i}(\boldsymbol{\kappa}_L \cdot \boldsymbol{X} + \sigma_L \tau_2)\}, \tag{4.20g}$$

$$\sigma_R = L^{(+)}_{\kappa_R i} + c_i + c_{aai}|\mathscr{A}_0|^2 + c_{bbi}|\mathscr{B}_0|^2, \tag{4.20h}$$

$$\sigma_L = L^{(-)}_{\kappa_L i} + c_i + c_{aai}|\mathscr{B}_0|^2 + c_{bbi}|\mathscr{A}_0|^2. \tag{4.20i}$$

From perturbations of this equilibrium state, we construct the linearized perturbation equations

$$A'_{\tau_2} = L^{(+)}A' + cA' + c_{aa}(A_0^2 A'^* + 2|\mathscr{A}_0|^2 A') + c_{bb}(A_0 B_0 B'^* + A_0 B_0^* B' + |\mathscr{B}_0|^2 A') + A_0 \boldsymbol{c}^{(+)}_p \cdot \nabla P', \tag{4.21a}$$

$$B'_{\tau_2} = L^{(-)}B' + cB' + c_{aa}(B_0^2 B'^* + 2|\mathscr{B}_0|^2 B') + c_{bb}(B_0 A_0 A'^* + B_0 A_0^* A' + |\mathscr{A}_0|^2 B') + B_0 \boldsymbol{c}^{(-)}_p \cdot \nabla P', \tag{4.21b}$$

$$0 = \tfrac{1}{3}\nabla^2 P' + \boldsymbol{c}^{(+)}_{rp} \cdot \nabla(A_0 A'^* + A_0^* A') + \boldsymbol{c}^{(-)}_{rp} \cdot \nabla(B_0 B'^* + B_0^* B'). \tag{4.21c}$$

These equations have solutions of the form

$$A' = (a^{(+)}E_k + a^{(-)}E_k^*)\,E_{\kappa_R}, \tag{4.22a}$$

$$B' = (b^{(+)}E_k + b^{(-)}E_k^*)\,E_{\kappa_L}, \tag{4.22b}$$

$$P' = p^{(+)}E_k + p^{(-)}E_k^*, \tag{4.22c}$$

where now $\boldsymbol{k} = (k, 0)$.

This two-dimensional disturbance also allows us to make a consistent transformation to a reference frame that moves with the mixed disturbance at the velocity $c_x \boldsymbol{e}_1$. The analysis proceeds in the usual fashion and results in the following characteristic equation for $\lambda$:

$$0 = \begin{vmatrix} f_{R+} + |\mathscr{A}_0|^2 f_{a+} - \lambda & \mathscr{A}_0^2 f_{a+} & \mathscr{A}_0 \mathscr{B}_0^* f_{b+} & \mathscr{A}_0 \mathscr{B}_0 f_{b+} \\ \mathscr{A}_0^{2*} f_{a+}^* & f_{R-}^* + |\mathscr{A}_0|^2 f_{a+}^* - \lambda & \mathscr{A}_0^* \mathscr{B}_0^* f_{b+}^* & \mathscr{A}_0^* \mathscr{B}_0 f_{b+}^* \\ \mathscr{B}_0 \mathscr{A}_0^* f_{b-} & \mathscr{B}_0 \mathscr{A}_0 f_{b-} & f_{L+} + |\mathscr{B}_0|^2 f_{a-} - \lambda & \mathscr{B}_0^2 f_{a-} \\ \mathscr{B}_0^* \mathscr{A}_0^* f_{b-}^* & \mathscr{B}_0^* \mathscr{A}_0 f_{b-}^* & \mathscr{B}_0^{2*} f_{a-}^* & f_{L-}^* + |\mathscr{B}_0|^2 f_{a-}^* - \lambda \end{vmatrix}, \tag{4.23a}$$

$$f_{R\pm} = L^{(+)}_{\kappa_R \pm k} - L^{(+)}_{\kappa_R}, \quad f_{L\pm} = L^{(-)}_{\kappa_L \pm k} - L^{(-)}_{\kappa_L}, \tag{4.23b, c}$$

$$f_{a\pm} = c_{aa} - \frac{3(\boldsymbol{c}_p^{(\pm)} \cdot \boldsymbol{k})\,(\boldsymbol{c}_{rp}^{(\pm)} \cdot \boldsymbol{k})}{|\boldsymbol{k}|^2}, \tag{4.23d}$$

$$f_{b\pm} = c_{bb} - \frac{3(\boldsymbol{c}_p^{(\pm)} \cdot \boldsymbol{k})\,(\boldsymbol{c}_{rp}^{(\mp)} \cdot \boldsymbol{k})}{|\boldsymbol{k}|^2}. \tag{4.23e}$$

With $\boldsymbol{k} = (k, 0)$ we have the simplification

$$f_{a\pm} = f_a = c_{aa} - 3c_{px}c_{rpx}, \quad f_{b\pm} = f_b = c_{bb} - 3c_{px}c_{rpx}. \tag{4.24a, b}$$

Note that one can show that the eigenvalues $\lambda$ computed from this determinant are independent of the phase of $\mathscr{A}_0$ and $\mathscr{B}_0$. Thus, we can evaluate the determinant by letting $\mathscr{A}_0$ and $\mathscr{B}_0$ be real.

Just as in the pure-wave case, we shall first investigate the long-wave disturbance. Setting $\boldsymbol{k} = \boldsymbol{0}$ in the determinant (4.23*a*), we obtain the characteristic equation

$$\lambda^2(\lambda^2 + p\lambda + q) = 0, \tag{4.25a}$$

$$p = -2(|\mathscr{A}_0|^2 + |\mathscr{B}_0|^2) f_{a_r}, \tag{4.25b}$$

$$q = 4|\mathscr{A}_0|^2|\mathscr{B}_0|^2(f_{a_r}^2 - f_{b_r}^2). \tag{4.25c}$$

Here, we have two zero roots corresponding to a neutrally stable phase disturbance for each of the components of the mixed wave, $A_0$ and $B_0$. A simple analysis shows that $\lambda_r > 0$ if $f_{a_r} > 0$, or if $f_{a_r} \leqslant 0$ and $f_{a_r}^2 - f_{b_r}^2 < 0$. Note that these relations are valid for every possible mixed-wave equilibrium state.

For the twelve parameter sets we have considered, we find that the mixed wave has an amplitude instability for each one except when $Bi = 1$ and $Pr = 0.001$ or $Pr = 0.01$. The two stable cases correspond to the same two cases in which a pure wave is unstable to a disturbance of the opposite kind, i.e. a pure right wave being unstable to a left-travelling disturbance. This suggests that the mixed-wave equilibrium state is the preferred waveform for these two parameter sets.

For the two cases in which the mixed wave is stable to an amplitude disturbance, we have the possibility of a sideband instability for non-zero values of $k$. To

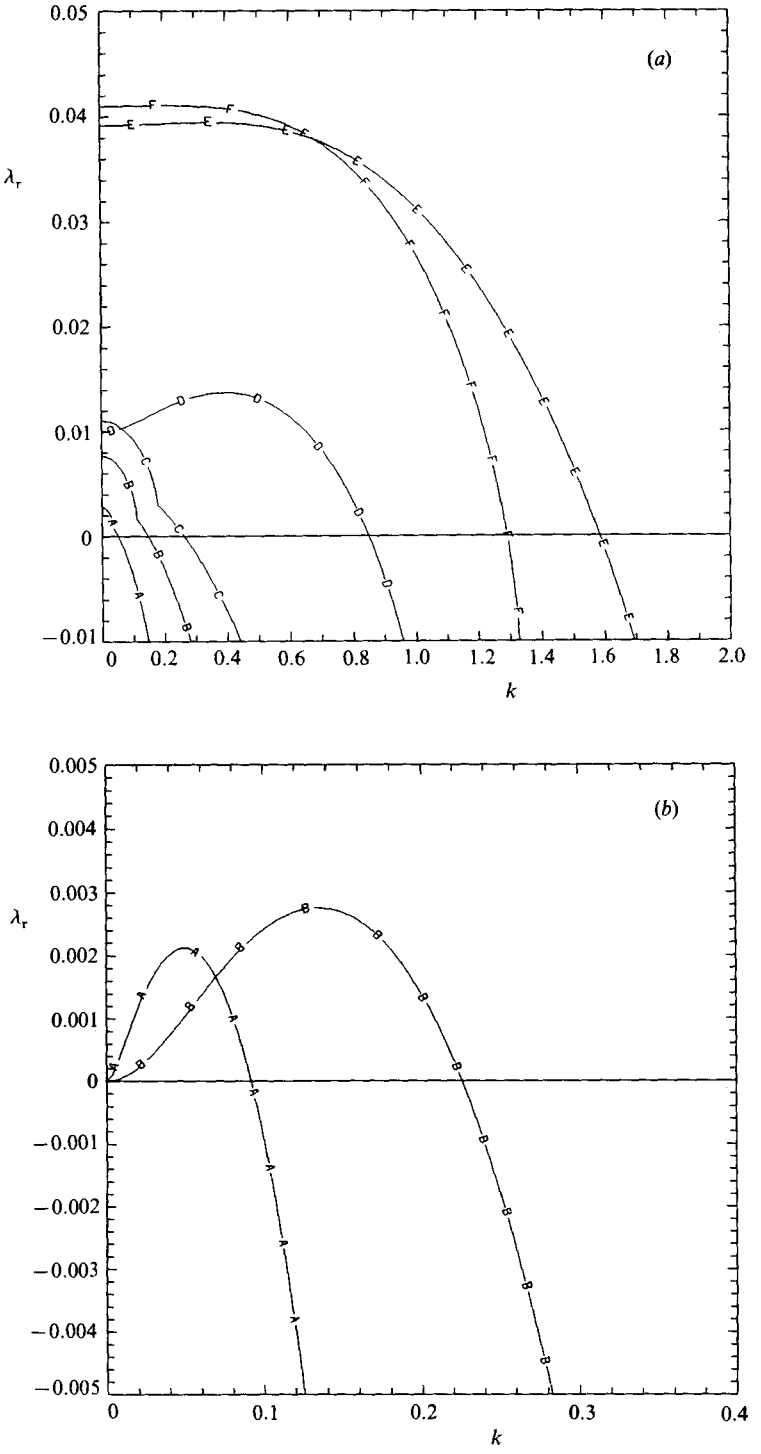


FIGURE 4 (*a*, *b*). For caption see facing page.

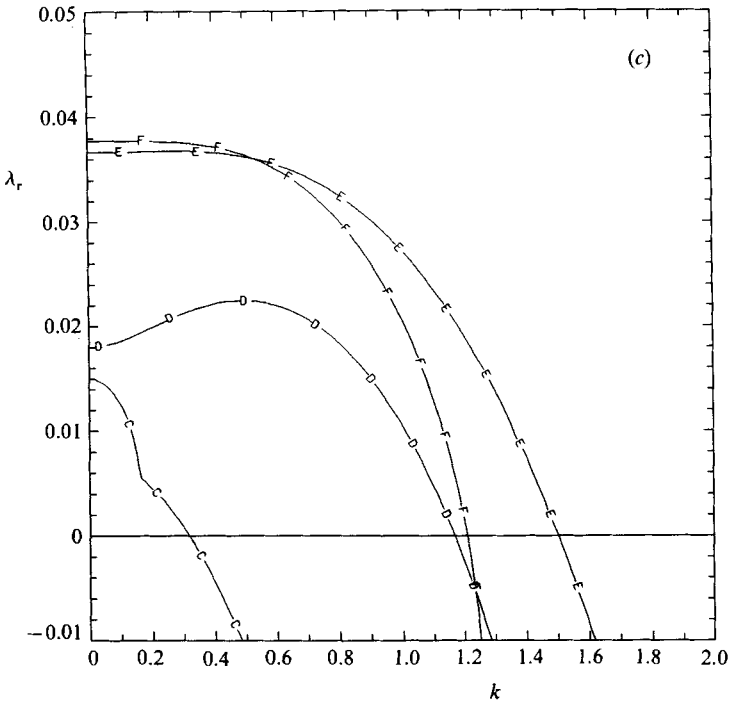


FIGURE 4. Curves of the growth rate of the sideband instability versus the disturbance wavenumber for a mixed wave with $\boldsymbol{\kappa}_R = \boldsymbol{\kappa}_L = \mathbf{0}$. (*a*) $Bi = 0$, (*b*) $Bi = 1$, and (*c*) $Bi = 1$. Curve A, $Pr = 0.001$; B, $Pr = 0.01$; C, $Pr = 0.1$; D, $Pr = 1.0$; E, $Pr = 10.0$; and F, $Pr = \infty$.

| | | | $Bi = 0$ | | | |
|---|---|---|---|---|---|---|
| $Pr$ | 0.001 | 0.01 | 0.1 | 1.0 | 10.0 | $\infty$ |
| $k$ | 0 | 0 | 0 | 0.394 | 0.340 | 0.209 |
| $\lambda_r$ | $0.277 \times 10^{-2}$ | $0.766 \times 10^{-2}$ | $0.110 \times 10^{-1}$ | $0.137 \times 10^{-1}$ | $0.395 \times 10^{-1}$ | $0.411 \times 10^{-1}$ |
| | | | $Bi = 1.0$ | | | |
| $Pr$ | 0.001 | 0.01 | 0.1 | 1.0 | 10.0 | $\infty$ |
| $k$ | 0.0499 | 0.135 | 0 | 0.494 | 0.275 | 0.0957 |
| $\lambda_r$ | $0.213 \times 10^{-2}$ | $0.275 \times 10^{-2}$ | $0.150 \times 10^{-1}$ | $0.225 \times 10^{-1}$ | $0.368 \times 10^{-1}$ | $0.377 \times 10^{-1}$ |

TABLE 4. The maximum value of the growth rate and the associated value of the wavenumber for the mixed wave with $\boldsymbol{\kappa}_R = \boldsymbol{\kappa}_L = \mathbf{0}$.

determine this, we must test whether $\lambda_r$, calculated from the determinant (4.23*a*) for all possible equilibrium wavevector pairs $\boldsymbol{\kappa}_R$ and $\boldsymbol{\kappa}_L$, is positive for any non-zero value of $k$. Here, the values of $\boldsymbol{\kappa}_R$ and $\boldsymbol{\kappa}_L$ were chosen on a (5pt, 10°) polar mesh superimposed on each of the elliptic regions of possible values for these wavenumbers. Again, we find that there is always a growing disturbance for any of the chosen equilibrium states. To illustrate this, we let $\boldsymbol{\kappa}_R = \boldsymbol{\kappa}_L = \mathbf{0}$ and plot the curves of $\lambda_r$ versus $k$ in figure 4(*a–c*). Curves A–F of figure 4(*a*) and curves C–F of figure 4(*c*) show that $\lambda_r > 0$ for $k = 0$ as shown earlier. In curves A and B of figure 4(*b*), we see that $\lambda_r = 0$ at $k = 0$ and so the instability is of the phase type for small values of $k$. The maximum value of $\lambda_r$ and the corresponding value of $k$ are shown in table 4.

## 5. Discussion

We have followed Benney & Newell (1967), Benney & Roskes (1969), and Newell & Whitehead (1969) in using the method of multiple scales to derive the evolution equations for the supercritical behaviour of the thermocapillary liquid-layer model. These equations include an explicit coupling to a pressure mode that was also recognized by Davey, Hocking & Stewartson (1974) for plane Poiseuille flow and by Hall (1984) for circular Couette flow. An immediate result of this pressure mode is the extra equation (3.14$g$). This equation is a generalized version of the one that appears in the work of Davey *et al.* (1974) because of the presence of the $Y_1$-derivatives on the wave amplitudes. These terms exist because the fundamental critical mode of the linear theory is three-dimensional. Thus, the system of evolution equations (3.11) and (3.14) is a further generalization of the Ginzburg–Landau equation to systems that exhibit a three-dimensional linear instability.

Physically, the pressure equation (3.14$g$) is a mass conservation law. The nonlinear interaction of the linear right wave with itself produces a mean streaming flow in the $x$- and $y$-directions of magnitude $|A|^2$. There is a similar flow of magnitude $|B|^2$ associated with linear left wave. When these mean streaming flows vary in magnitude over the long lengthscales used in this study, the system must develop an additional flow in order to maintain mass conservation. This additional flow is driven by a long-range pressure gradient $\hat{\boldsymbol{\nabla}}_1 P$ which develops in the layer. Equation (3.14$g$) is the mathematical expression of mass conservation between this pressure-driven flow and the nonlinear streaming flows. The long-range pressure gradient is analogous to the basic-state pressure gradient that is set up by the slot ends in order to ensure that the net mass flux of the basic-state velocity profile is zero.

In a similar manner, the heat flux condition (3.11$e$) represents an energy balance in the layer on the long lengthscale. The three terms on the right-hand side of this equation are the heat fluxes due to the mean streaming flows produced by the long-range pressure gradient and the nonlinear self-interactions of the linear right and left waves respectively. To balance these fluxes when $Bi \neq 0$ a heat flux into the top of the layer is produced by the system. When $Bi = 0$, the system cannot produce a flux and we must impose it from the outside. Thus, we do not really have an insulated top surface in this limit. In imposing this flux $Q$, we essentially impose the condition that the average temperature perturbation in the layer is zero.

If we set $Q = 0$, the limit $Bi \to 0$ corresponds exactly to a completely insulated top surface. The energy balance in the layer will then be maintained if we let the average temperature in the layer evolve with the instability. The heat flux equation (3.11$e$) now becomes an evolution equation for the amplitude of the temperature eigenfunction $C$ which was defined in equation (3.8$a$). The temperature also couples with the evolution equations (3.14$a, b$) for the wave amplitudes. This more complicated set of equations is written in Appendix D. The stability behaviour of equilibrium solutions governed by this set of equations will be examined in a future publication.

The stability analysis presented in the previous section follows the work of Stuart & DiPrima (1978), who considered only two-dimensional perturbations to the Ginzburg–Landau equation, and the work of Holmes (1985), who generalized the previous analysis to three-dimensional disturbances and included the coupling to the pressure mode. These previous analyses were able to obtain some explicit inequalities for instability based on locating the extremum of the characteristic equation. Finding such inequalities is probably hopeless in this study because of the complexity

of the characteristic equations which we have expressed as the determinants (4.17*a*) and (4.23*a*). Thus, we determine instability by the straightforward method of maximizing the growth rate $\lambda_r$ for each possible equilibrium state with respect to all possible disturbance wavenumbers, and then determining if $\lambda_r > 0$.

Note that our results show singular behaviour in the limit of $\boldsymbol{k} \to \boldsymbol{0}$. This is signalled by the disappearance of the term $\nabla^2 P'$ in (4.11*c*) and (4.21*c*) in this limit. Thus, the pressure mode must be taken into account even in the study of uniform disturbances to an equilibrium solution. Furthermore, (4.17*c*) shows that the value of $f_{a\pm}$ depends on which direction the small-$\boldsymbol{k}$ limit is taken. This type of behaviour is also seen in the work of Holmes (1985).

The results of the stability analysis of §4 must be carefully considered in the light of the types of instabilities that were predicted. Our first result concerns 'amplitude' instability which is described in the limit of $\boldsymbol{k} \to \boldsymbol{0}$. We find that a subset of the possible pure-wave equilibrium states is 'amplitude' stable for all of the parameter sets considered here, except for $Bi = 1$ and $Pr = 0.001$ or $Pr = 0.01$. This result is shown in figure 2(*a–f*). To explain these figures, consider any possible pure-$A$ equilibrium state. The nonlinear interactions of the pure-$A$ wave with a $B'$-disturbance causes a stabilization of the disturbance if the amplitude of the pure-$A$ wave is large enough. The amplitude is highest at the centre of the elliptical region of possible equilibrium states and decreases toward the boundary as shown in equation (4.9*d*). Thus, near the boundary the amplitude of the pure-$A$ wave is not large enough to effect the stabilization and the $B'$-disturbance grows in amplitude. Near the centre of the ellipse, the stabilization does occur and the pure-$A$ wave is 'amplitude' stable. For $Bi = 1$ and $Pr = 0.001$ or $Pr = 0.01$, the interaction coefficient $c_{bb}$ is not large enough to cause the stabilization of the $B'$-disturbance even for the largest pure-$A$ amplitude. Thus, the $B'$–disturbance always grows.

We have also seen that all possible mixed-wave-equilibrium states have an 'amplitude' instability for all of the parameter sets considered here, except when $Bi = 1$ and $Pr = 0.001$ or $Pr = 0.01$. Examination of the mixed-wave eigenfunction for these unstable modes reveals that the $A'$-part and the $B'$-part have opposite signs. This says that one of the parts will increase and the other will decrease depending on which one is larger initially. Such behaviour destroys the mixed character of the mixed-wave equilibrium state. This result indicates that for the ten parameter sets that predict pure-wave 'amplitude' stability and mixed-wave 'amplitude' instability, the system should develop into some form of a pure wave. Once a pure wave has formed, any perturbation to it that is of the opposite type will decay.

Likewise, when $Bi = 1$ and $Pr = 0.001$ or $Pr = 0.01$ all of the mixed-wave equilibrium states exhibit 'amplitude' stability and the pure-wave equilibrium states exhibit 'amplitude' instability. Thus, we expect the system to develop into some form of a mixed wave.

For the specific equilibrium states studied in this work with $\boldsymbol{\kappa}_R = \boldsymbol{\kappa}_L = \boldsymbol{0}$, we find what Kuramoto (1984) calls a phase instability. This instability corresponds to that eigenvalue which approaches zero as the magnitude of the disturbance wavenumber becomes small. In this limit, the system of evolution equations (3.14) is invariant to a change in the phase of the solution because the nonlinear terms in the system are actually linear in the phase of $A$ and $B$. Thus, a constant-phase disturbance is neutrally stable. Near this limit point, one would expect the disturbance to mostly affect the phase of the equilibrium state. As the wavenumber increases, however, this distinction should disappear.

For all possible equilibrium states we found an instability whose most dangerous disturbance did not generally occur at $\boldsymbol{k} = \boldsymbol{0}$. The form of the disturbances used in the analysis shows that we actually have another case of the Eckhaus and Benjamin–Feir sideband instability. As described clearly by Stuart & DiPrima (1978), the mechanism for this instability is essentially a resonance between two disturbances (the sideband modes) set up by the nonlinear interactions of the disturbances with the first harmonic of the fundamental linear wave.

The equilibrium states considered in this paper represent coherent plane waves. In predicting a sideband instability for both the pure wave and the mixed wave, we expect a loss of coherence for these equilibrium states. Thus, the relative phasing of the wavefronts and their amplitudes will become modified on the long length- and timescales used in this analysis. The actual spatial and temporal development can be described by integration of the evolution equations directly. We would expect behaviour similar to the chaotic solutions described by Moon, Huerre & Redekopp (1983) for the Ginzburg–Landau equation and the intermittent behaviour described by Bretherton & Spiegel (1983).

When $Bi = 0$, the evolution heat equation (3.11*e*) was ignored in our stability analysis of the nonlinear evolution equations since it decoupled from the others. This equation shows that for all of the equilibrium states considered in this study, the heat flux is out of or into the layer depending on whether the sign of the constant $\mu$ is positive or negative. For the six relevant parameter sets considered in this work, $\mu$ is always negative. Thus, there is always a net heat flux *into* the layer owing to the nonlinear interactions of the unstable linear waves in these equilibrium states.

When $Bi \neq 0$, we examine the heat flux to the layer by considering the mean response of the liquid due to the nonlinear interactions. For $Bi = 1$, we find that there is also a mean heat flux into the layer for all values of the Prandtl number considered. This result expresses the fact that the energy needed to sustain the nonlinear equilibrium state must be obtained from the environment by heat transfer through the top surface of the layer.

## 6. Conclusions

The stability of a liquid layer driven by the thermocapillary effect of a temperature gradient imposed on its upper free surface has been examined. The linear theory of SD has shown that two hydrothermal waves become unstable at the same time. One moves backward and to the right and the other moves backward and to the left. Their data has been supplemented in this work by further calculations for the critical Marangoni number, the critical wavenumber vector, and the critical frequency at the onset of the instability for a full range of Prandtl numbers and $Bi = 1$.

A weakly nonlinear, multiple-scale analysis was used to develop the set of nonlinear evolution equations (3.11) and (3.14) for this instability. These equations, a generalized version of the Ginzburg–Landau equation, couple the modal amplitudes of the unstable right and left linear waves, the associated pressure field, and a surface heat flux when $Bi = 0$. The stability of two sets of possible equilibrium states for these evolution equations was carefully examined. The first set is the pure-wave state consisting of either the right or the left linear wave. The second set is the mixed-wave state which is a combination of the both of the linear waves. It was found that a subset of the possible pure-wave states is stable to amplitude perturbations for all the parameter sets considered except for $Bi = 1$ and $Pr = 0.001$ or $Pr = 0.01$. For these two parameter sets, the mixed wave is stable to amplitude perturbations, but it is

unstable for the others. Thus, we expect the system to develop into a pure-wave state except when $Bi$ is near one and $Pr \leqslant 0.01$. In this parameter range, the system should develop into a mixed-wave state.

Our analysis also shows that all of these equilibrium states exhibit a sideband instability. This suggests that they will lose their spatial coherence as they become modulated on both long space and times scales. The wavenumber vector and growth rate of the fastest growing sideband instability for one pure-wave case and one mixed-wave case are tabulated in tables 3 and 4.

We expect the above results to serve as a rough guide to the behaviour of the thermocapillary instability that appears in the finite cylindrical geometry of present float-zone experiments. The experiments by Chun & Wuest (1979), Preisser, Schwabe & Scharmann (1983), and Kamotani, Ostrach & Vargas (1984) all find an instability that propagates azimuthally around the cylinder. Such a motion is consistent with the obliquely travelling hydrothermal wave of the planar model or the spiralling hydrothermal wave found in the infinite-cylinder model by Xu & Davis (1984). In all of these experiments, a working fluid with a relatively large Prandtl number was used and so the results are consistent with the predictions of this nonlinear theory. However, these experiments are meant to model the instability in a float zone of liquid silicon. The Prandtl number of liquid silicon is 0.023 and since the Biot number of an actual zone is not close to zero, this analysis suggests that a mixed wave might be the preferred waveform for the instability. If this is true, the experiments may not be an appropriate model for a silicon float zone. We could do further calculations that precisely define the boundary between a pure wave and a mixed wave in ($Pr$, $Bi$)-space, but these would not be very useful since, as we said earlier, our results can only serve as a rough guide to the actual experiments.

The nonlinear interactions of the fundamental unstable linear wave produce a mean heat flux into the layer from the outside environment. This prediction could be used as a means of characterizing the onset of the instability in an experiment. It is analogous to the increase in the torque that signals the onset of Taylor vortices in concentric rotating cylinders.

This work was supported by the National Science Foundation, Grant No. MSM-8451093. The author acknowledges a helpful discussion with Dr M. R. E. Proctor during the course of this work. The figures in this paper were drawn using the NCAR graphics system.

## Appendix A. Operator definitions

The differential operators and vectors used in system (3.2) are defined as follows:

$$\mathbf{L} = \begin{bmatrix} \nabla^2 - MPr^{-1}\left\{\dfrac{\partial}{\partial t} + \bar{u}\dfrac{\partial}{\partial x} + \boldsymbol{e}_1(\bar{u}_z \boldsymbol{e}_3 \cdot)\right\} & -\nabla & 0 \\ \nabla\cdot & 0 & 0 \\ -M\{\bar{T}_x \boldsymbol{e}_1 + \bar{T}_z \boldsymbol{e}_3\}. & 0 & \nabla^2 - M\left\{\dfrac{\partial}{\partial t} + \bar{u}\dfrac{\partial}{\partial x}\right\} \end{bmatrix}, \quad \text{(A 1}a\text{)}$$

$$\mathbf{B}_0 = \begin{bmatrix} 1 & 0 & 0 \\ 0 & 0 & \dfrac{\partial}{\partial z} \end{bmatrix}, \quad \text{(A 1}b\text{)}$$

$$\mathbf{B}_1 = \begin{bmatrix} \boldsymbol{e}_1\frac{\partial}{\partial z}(\boldsymbol{e}_1\cdot)+\boldsymbol{e}_2\frac{\partial}{\partial z}(\boldsymbol{e}_2\cdot)+\boldsymbol{e}_3(\boldsymbol{e}_3\cdot) & 0 & \boldsymbol{e}_1\frac{\partial}{\partial x}+\boldsymbol{e}_2\frac{\partial}{\partial y} \\ 0 & 0 & \frac{\partial}{\partial z}+Bi \end{bmatrix}, \tag{A 1c}$$

$$\mathcal{Q} = \{\mathbf{0}, 0, Q\}^{\mathrm{T}}, \quad \mathcal{N} = \{Pr^{-1}(\boldsymbol{v}\cdot\nabla)\boldsymbol{v}, 0, \boldsymbol{v}\cdot\nabla T\}^{\mathrm{T}}. \tag{A 1d, e}$$

Here $\boldsymbol{e}_2$ and $\boldsymbol{e}_3$ are unit vectors in the $y$- and $z$-directions respectively.

After expanding the derivatives of $x$, $y$ and $t$ that appear in the operators (A 1) with respect to the multiple scales defined by system (3.4) and substituting the expansion for $M$ from (3.3) into the operator $\mathbf{L}$, we obtain the following:

$$\mathbf{L} = \mathbf{L}^{(0)}+\epsilon\mathbf{L}^{(1)}+\epsilon^2\mathbf{L}^{(2)}+\ldots, \tag{A 2a}$$

$$\mathbf{B}_1 = \mathbf{B}_1^{(0)}+\epsilon\mathbf{B}_1^{(1)}+\epsilon^2\mathbf{B}_1^{(2)}+\ldots. \tag{A 2b}$$

These operators are written as follows.

$$\mathbf{L}^{(0)} = \begin{bmatrix} \nabla^2-M_{\mathrm{c}}Pr^{-1}\left\{\frac{\partial}{\partial t}+\bar{u}\frac{\partial}{\partial x}+\boldsymbol{e}_1(\bar{u}_z\boldsymbol{e}_3\cdot)\right\} & -\nabla & 0 \\ \nabla\cdot & 0 & 0 \\ -M_{\mathrm{c}}\{\bar{T}_x\boldsymbol{e}_1+\bar{T}_z\boldsymbol{e}_3\}\cdot & 0 & \nabla^2-M_{\mathrm{c}}\left\{\frac{\partial}{\partial t}+\bar{u}\frac{\partial}{\partial x}\right\} \end{bmatrix}, \tag{A 3}$$

$$\mathbf{L}^{(1)} = \frac{\partial}{\partial X_1}\mathbf{L}_X+\frac{\partial}{\partial Y_1}\mathbf{L}_Y+\frac{\partial}{\partial \tau_1}\mathbf{L}_\tau, \tag{A 4a}$$

$$\mathbf{L}_X = \begin{bmatrix} 2\frac{\partial}{\partial x}-M_{\mathrm{c}}Pr^{-1}\bar{u} & -\boldsymbol{e}_1 & 0 \\ \boldsymbol{e}_1\cdot & 0 & 0 \\ 0 & 0 & 2\frac{\partial}{\partial x}-M_{\mathrm{c}}\bar{u} \end{bmatrix}, \tag{A 4b}$$

$$\mathbf{L}_Y = \begin{bmatrix} 2\frac{\partial}{\partial y} & -\boldsymbol{e}_2 & 0 \\ \boldsymbol{e}_2\cdot & 0 & 0 \\ 0 & 0 & 2\frac{\partial}{\partial y} \end{bmatrix}, \tag{A 4c}$$

$$\mathbf{L}_\tau = \begin{bmatrix} -M_{\mathrm{c}}Pr^{-1} & 0 & 0 \\ 0 & 0 & 0 \\ 0 & 0 & -M_{\mathrm{c}} \end{bmatrix}, \tag{A 4d}$$

$$\mathbf{L}^{(2)} = \frac{\partial}{\partial X_2}\mathbf{L}_X+\frac{\partial}{\partial Y_2}\mathbf{L}_Y+\frac{\partial}{\partial \tau_2}\mathbf{L}_\tau+\nabla_1^2\mathbf{L}_\nabla+\mathbf{L}_M, \tag{A 5a}$$

$$\mathbf{L}_\nabla = \begin{bmatrix} 1 & 0 & 0 \\ 0 & 0 & 0 \\ 0 & 0 & 1 \end{bmatrix}, \tag{A 5b}$$

$$\mathbf{L}_M = \begin{bmatrix} -M_c Pr^{-1}\left\{\dfrac{\partial}{\partial t}+\bar{u}\dfrac{\partial}{\partial x}+\boldsymbol{e}_1(\bar{u}_z\boldsymbol{e}_3\cdot)\right\} & 0 & 0 \\ 0 & 0 & 0 \\ -M_c\{\bar{T}_x\boldsymbol{e}_1+2\bar{T}_z\boldsymbol{e}_3\}\cdot & 0 & -M_c\left\{\dfrac{\partial}{\partial t}+\bar{u}\dfrac{\partial}{\partial x}\right\} \end{bmatrix}. \tag{A 5c}$$

The boundary-condition operators are defined as follows:

$$\mathbf{B}_1^{(0)} = \begin{bmatrix} \boldsymbol{e}_1\dfrac{\partial}{\partial z}(\boldsymbol{e}_1\cdot)+\boldsymbol{e}_2\dfrac{\partial}{\partial z}(\boldsymbol{e}_2\cdot)+\boldsymbol{e}_3(\boldsymbol{e}_3\cdot) & 0 & \boldsymbol{e}_1\dfrac{\partial}{\partial x}+\boldsymbol{e}_2\dfrac{\partial}{\partial y} \\ 0 & 0 & \dfrac{\partial}{\partial z}+Bi \end{bmatrix}, \tag{A 6}$$

$$\mathbf{B}_1^{(1)} = \frac{\partial}{\partial X_1}\mathbf{B}_X+\frac{\partial}{\partial Y_1}\mathbf{B}_Y, \tag{A 7a}$$

$$\mathbf{B}_1^{(2)} = \frac{\partial}{\partial X_2}\mathbf{B}_X+\frac{\partial}{\partial Y_2}\mathbf{B}_Y, \tag{A 7b}$$

$$\mathbf{B}_X = \begin{bmatrix} 0 & 0 & \boldsymbol{e}_1 \\ 0 & 0 & 0 \end{bmatrix}, \tag{A 7c}$$

$$\mathbf{B}_Y = \begin{bmatrix} 0 & 0 & \boldsymbol{e}_2 \\ 0 & 0 & 0 \end{bmatrix}, \tag{A 7d}$$

The expansion of the nonlinear vector is given as follows:

$$\mathcal{N}^{(2)} = \{Pr^{-1}(\boldsymbol{v}^{(1)}\cdot\nabla)\,\boldsymbol{v}^{(1)},\ 0,\ \boldsymbol{v}^{(1)}\cdot\nabla T^{(1)}\}^{\mathrm{T}}, \tag{A 8a}$$

$$\mathcal{N}^{(3)} = \{Pr^{-1}[(\boldsymbol{v}^{(1)}\cdot\nabla)\,\boldsymbol{v}^{(2)}+(\boldsymbol{v}^{(2)}\cdot\nabla)\,\boldsymbol{v}^{(1)}],\ 0,\ (\boldsymbol{v}^{(1)}\cdot\nabla T^{(2)}+\boldsymbol{v}^{(2)}\cdot\nabla T^{(1)})\}^{\mathrm{T}}. \tag{A 8b}$$

## Appendix B. Details of the multiple-scales problem

Using the expansions defined in (3.5) on the system of equations (3.2), we obtain the following sequence of problems to be solved:

at $O(\epsilon)$,

$$\mathbf{L}^{(0)}\boldsymbol{\Psi}^{(1)} = \mathbf{0}, \tag{B 1a}$$

$$\mathbf{B}_0\,\boldsymbol{\Psi}^{(1)} = \mathbf{0} \quad \text{on } z=0, \tag{B 1b}$$

$$\mathbf{B}_1^{(0)}\boldsymbol{\Psi}^{(1)} = \mathbf{0} \quad \text{on } z=1; \tag{B 1c}$$

at $O(\epsilon^2)$,

$$\mathbf{L}^{(0)}\boldsymbol{\Psi}^{(2)} = -\mathbf{L}^{(1)}\boldsymbol{\Psi}^{(1)}+M_c\mathcal{N}^{(2)}, \tag{B 2a}$$

$$\mathbf{B}_0\,\boldsymbol{\Psi}^{(2)} = \mathbf{0} \quad \text{on } z=0, \tag{B 2b}$$

$$\mathbf{B}_1^{(0)}\boldsymbol{\Psi}^{(2)} = -\mathbf{B}_1^{(1)}\boldsymbol{\Psi}^{(1)}-\boldsymbol{Q}^{(2)} \quad \text{on } z=1; \tag{B 2c}$$

at $O(\epsilon^3)$,

$$\mathbf{L}^{(0)}\boldsymbol{\Psi}^{(3)} = -\mathbf{L}^{(1)}\boldsymbol{\Psi}^{(2)}-\mathbf{L}^{(2)}\boldsymbol{\Psi}^{(1)}+M_c\mathcal{N}^{(3)}, \tag{B 3a}$$

$$\mathbf{B}_0\,\boldsymbol{\Psi}^{(3)} = \mathbf{0} \quad \text{on } z=0, \tag{B 3b}$$

$$\mathbf{B}_1^{(0)}\boldsymbol{\Psi}^{(3)} = -\mathbf{B}_1^{(1)}\boldsymbol{\Psi}^{(2)}-\mathbf{B}_1^{(2)}\boldsymbol{\Psi}^{(1)}-\boldsymbol{Q}^{(3)} \quad \text{on } z=1. \tag{B 3c}$$

The solution of the $O(\epsilon)$ problem was given in general terms in (3.6). The critical right wave in normal-mode form is

$$\boldsymbol{\Psi}_{\mathrm{R}}^{(1)} = A\hat{\boldsymbol{\Psi}}_{\mathrm{R}}^{(1)}(z)\exp\{\mathrm{i}(\boldsymbol{k}_{\mathrm{c}}^{(+)}\cdot\boldsymbol{x}+\omega_{\mathrm{c}}t)\}+\mathrm{c.c.} \tag{B 4}$$

Here, $A = A(X_1, X_2, Y_1, Y_2, \tau_1, \tau_2)$ is the complex amplitude of the normal-mode eigenfunction $\hat{\boldsymbol{\Psi}}_{\mathrm{R}}^{(1)}(z)$, $\boldsymbol{k}_{\mathrm{c}}^{(+)} = (k_{\mathrm{c}1}, k_{\mathrm{c}2})$ is the critical wavenumber vector, $\omega_{\mathrm{c}}$ is the frequency at the critical point, and c.c. is the complex conjugate of the first term. The critical left wave in normal-mode form is

$$\boldsymbol{\Psi}_{\mathrm{L}}^{(1)} = B\hat{\boldsymbol{\Psi}}_{\mathrm{L}}^{(1)}(z)\exp\{\mathrm{i}(\boldsymbol{k}_{\mathrm{c}}^{(-)}\cdot\boldsymbol{x}+\omega_{\mathrm{c}}t)\}+\mathrm{c.c.}, \tag{B 5}$$

where $B = B(X_1, X_2, Y_1, Y_2, \tau_1, \tau_2)$ and $\boldsymbol{k}_{\mathrm{c}}^{(-)} = (k_{\mathrm{c}1}, -k_{\mathrm{c}2})$.

The inhomogeneous boundary-value problems above are solved by first transferring the inhomogeneous term in the boundary conditions to the differential equations. This allows for an easier construction of the adjoint problem.

The orthogonality condition is an inner product of two vectors, $\boldsymbol{f}$ and $\boldsymbol{g}$ say, and is defined as

$$\langle \boldsymbol{f}, \boldsymbol{g}\rangle = \frac{1}{2\pi/\omega_{\mathrm{c}}}\frac{1}{V}\int_0^{2\pi/\omega_{\mathrm{c}}}\int_V \boldsymbol{f}\cdot\boldsymbol{g}\,\mathrm{d}V\,\mathrm{d}t, \tag{B 6}$$

where $V = \int_V \mathrm{d}V$ and $2\pi/\omega_{\mathrm{c}}$ is the period of oscillation of the critical linear waves.

## Appendix C. Local geometry

The geometry of the neutral surface and the frequency surface at the critical point is related to the linear coefficients of the evolution equations (3.11) and (3.14) by the following relations:

$$c = M_{\mathrm{c}}\left\{-\frac{\partial\omega_{\mathrm{i}}}{\partial M}+\mathrm{i}\frac{\partial\omega_{\mathrm{r}}}{\partial M}\right\} = \mathrm{i}M_{\mathrm{c}}\frac{\partial\omega}{\partial M}, \tag{C 1$a$}$$

$$c_x = -\frac{\partial\omega}{\partial k_1}, \tag{C 1$b$}$$

$$c_y = -\frac{\partial\omega}{\partial k_2}, \tag{C 1$c$}$$

$$c_{xx} = -\frac{\mathrm{i}}{2}\frac{\partial^2\omega}{\partial k_1^2}+\frac{c}{2M_{\mathrm{c}}}\frac{\partial^2 M}{\partial k_1^2}, \tag{C 1$d$}$$

$$c_{xy} = -\mathrm{i}\frac{\partial^2\omega}{\partial k_1\partial k_2}+\frac{c}{M_{\mathrm{c}}}\frac{\partial^2 M}{\partial k_1\partial k_2}, \tag{C 1$e$}$$

$$c_{yy} = -\frac{\mathrm{i}\partial^2\omega}{2\partial k_2^2}+\frac{c}{2M_{\mathrm{c}}}\frac{\partial^2 M}{\partial k_2^2}. \tag{C 1$f$}$$

In (C 1$a$), $\omega$ is evaluated with respect to a change in $M$, i.e. stepping off the neutral surface. Thus, it becomes complex due to the instability of the linear problem above the neutral surface. In the rest of the equations, $\omega$ is evaluated with respect to a change in the wavenumber along the neutral surface. Thus, $\omega$ is always real.

## Appendix D. Alternative evolution equations

As explained in §5, when $Bi = 0$ we can set $Q = 0$ and derive an alternative set of evolution equations for this system. Here, the amplitude $C$ of the temperature eigenfunction defined in (3.8*a*) evolves on the long length- and timescales. These equations are given as follows:

$$A_{\tau_2} + \boldsymbol{c}_{\mathrm{g}}^{(+)} \cdot \hat{\boldsymbol{\nabla}}_2 A = \hat{L}^{(+)} A + cA + A[c_{aa}|A|^2 + c_{bb}|B|^2] + A\boldsymbol{c}_p^{(+)} \cdot \hat{\boldsymbol{\nabla}}_1 P + A\boldsymbol{c}_{\mathrm{c}}^{(+)} \cdot \hat{\boldsymbol{\nabla}}_1 C, \quad \text{(D 1}a\text{)}$$

$$B_{\tau_2} + \boldsymbol{c}_{\mathrm{g}}^{(-)} \cdot \hat{\boldsymbol{\nabla}}_2 B = \hat{L}^{(-)} B + cB + B[c_{aa}|B|^2 + c_{bb}|A|^2] + B\boldsymbol{c}_p^{(-)} \cdot \hat{\boldsymbol{\nabla}}_1 P + B\boldsymbol{c}_{\mathrm{c}}^{(-)} \cdot \hat{\boldsymbol{\nabla}}_1 C, \quad \text{(D 1}b\text{)}$$

$$C_{\tau_1} = \tfrac{1}{2}\bar{T}_x C_{X_1} + \tfrac{1}{3}\bar{T}_x P_{X_1} + \mu(|A|^2 + |B|^2), \quad \text{(D 1}c\text{)}$$

$$0 = \tfrac{1}{2}\hat{\nabla}_1^2 C + \tfrac{1}{3}\hat{\nabla}_1^2 P + \boldsymbol{c}_{rp}^{(+)} \cdot \hat{\boldsymbol{\nabla}}_1 |A|^2 + \boldsymbol{c}_{rp}^{(-)} \cdot \hat{\boldsymbol{\nabla}}_1 |B|^2, \quad \text{(D 1}d\text{)}$$

where

$$\boldsymbol{c}_{\mathrm{c}}^{(\pm)} = c_{cx}\boldsymbol{e}_1 \pm c_{cy}\boldsymbol{e}_2. \quad \text{(D 1}e\text{)}$$

The coefficients $c_{cx}$ and $c_{cy}$ have not been calculated in this work.

## REFERENCES


Benjamin, T. B. & Feir, J. E. 1967 *J. Fluid Mech.* **27**, 417.

Benney, D. J. & Newell, A. C. 1967 *J. Math. Phys.* **46**, 133.

Benney, D. J. & Roskes, G. J. 1969 *Stud. Appl. Maths* **48**, 377.

Bretherton, C. S. & Spiegel, E. A. 1983 *Phys. Lett.* **96A**, 152.

Chun, C.-H. & Wuest, W. 1979 *Acta Astronaut.* **6**, 1073.

Davey, A., Hocking, L. M. & Stewartson, K. 1974 *J. Fluid Mech.* **63**, 529.

Davis, S. H. 1987 *Ann. Rev. Fluid Mech.* **19**, 403.

Davis, S. H. & Homsy, G. M. 1980 *J. Fluid Mech.* **98**, 527.

Davis, S. H. & Segel, L. A. 1968 *Phys. Fluids* **11**, 470.

Eckhaus, W. 1965 *Studies in Non-Linear Stability Theory*. Springer.

Hall, P. 1984 *Phys. Rev.* **A29**, 2921.

Holmes, C. A. 1985 *Proc. R. Soc. Lond.* **A402**, 299.

Kamotani, Y., Ostrach, S. & Vargas, M. 1984 *J. Cryst. Growth* **66**, 83.

Kenning, D. B. R. 1968 *Appl. Mech. Rev.* **21**, 1101.

Kuramoto, Y. 1984 *Chemical Oscillations, Waves, and Turbulence*. Springer.

Moon, H. T., Huerre, P. & Redekopp, L. G. 1983 *Physica* **7D**, 135.

Newell, A. C. & Whitehead, J. A. 1969 *J. Fluid Mech.* **38**, 279.

Preisser, F., Schwabe, D. & Scharmann, A. 1983 *J. Fluid Mech.* **126**, 545.

Sani, R. 1964 *J. Fluid Mech.* **20**, 315.

Scriven, L. E. & Sternling, C. V. 1960 *Nature* **187**, 186.

Scott, M. R. & Watts, H. A. 1975 *Rep.* SAND 75-0198. Sandia Labs, Alburquerque, NM.

Scott, M. R. & Watts, H. A. 1977 *SIAM J. Numer. Anal.* **14**, 40.

Sen, A. K. & Davis, S. H. 1982 *J. Fluid Mech.* **121**, 163.

Smith, M. K. 1986 *Phys. Fluids* **29**, 3182.

Smith, M. K. & Davis, S. H. 1983 *J. Fluid Mech.* **132**, 119.

Stuart, J. T. & DiPrima, R. C. 1978 *Proc. R. Soc. Lond.* **A362**, 27.

Xu, J. J. & Davis, S. H. 1984 *Phys. Fluids* **27**, 1102.